A complete process for production of flexible large area polymer solar cells entirely using screen printing—First public demonstration

Frederik C. Krebs [a,*], Mikkel Jørgensen [a], Kion Norrman [a], Ole Hagemann [a], Jan Alstrup [a], Torben D. Nielsen [a], Jan Fyenbo [b], Kaj Larsen [b], Jette Kristensen [b]

[a] Risø National Laboratory for Sustainable Energy, Technical University of Denmark, Frederiksborgvej 399, DK-4000 Roskilde, Denmark
[b] Mekoprint Electronics, Hermesvej 4, DK-9530 Støvring, Denmark

ARTICLE INFO

ABSTRACT

A complete polymer solar cell module prepared in the ambient atmosphere under industrial conditions is presented. The versatility of the polymer solar cell technology is demonstrated through the use of abstract forms for the active area, a flexible substrate, processing entirely from solution, complete processing in air using commonly available screen printing, and finally, simple mechanical encapsulation using a flexible packaging material and electrical contacting post-production using crimped contacts. We detail the production of more than 2000 modules in one production run and show that the production technique is scalable and well suited for direct transfer to the printing industry employing existing production equipment. The production speed and cost analysis for the individual modules from this batch is discussed and a forecast for the high volume cost based on this method is given. Further, the points where significant cost reductions can be achieved are identified. The use of the solar cell as the power supply for a small radio and other small electronic circuits is demonstrated. Lastly, the operational stability under ambient conditions in the dark and under illumination is discussed.

© 2008 Elsevier B.V. All rights reserved.

1. Introduction

1.1. Polymer solar cells—a brief overview

Solar cells based on polymer materials [1–8] could in principle offer production in high volume at low process cost. Research on the subject has focussed mainly on improving the power conversion efficiency for small laboratory cells [9–11] through optimization of materials and the protocol used for preparation. Meanwhile the vision of fast, low-temperature solution processing has been used as a justification for the research activity. The equally important areas of stability [8] and processing into large modules [12–14] have been given very little attention. It is of importance to investigate both the operational stability that can be achieved under ideal conditions where the sources of degradation have been removed or excluded from the experiment [15–17], but also the operational stability that is practically achieved for a given material combination under a given set of conditions [18–22]. It is equally important to attempt large-scale production to affirm the likely benefits the technology may have

to offer in terms of processing ease and cost. Currently there is no clear view of the final choice of the processing method(s) for polymer solar cells and it is likely that several different approaches are going to be employed to begin with, and that these may evolve into one preferred method for a given class of materials and devices. Since the choice of polymer material is essentially infinite it is highly likely that many different types of polymer solar cells processed by widely different methods will come in to existence, some of which may be viable commercially.

1.2. Cost analysis of polymer solar cells

In the high volume approximation considerations of the process cost and the material cost become important. While no rigid analysis has been made so far, several projections relating to the overall cost can be made. There are general concerns on the environmental consequences for large-scale production and distribution of low-cost solar cells. There is a risk of causing more harm to the environment than the benefits gained by using the solar power from them. The cost analysis of polymer solar cells thus necessarily has to include an evaluation of the impact the production and the product has on the surroundings. This implies that the simplest and least harmful production process

---

and conditions should be sought. To underline this train of thought; a highly efficient polymer solar cell technology that implies the use of expensive/scarce/toxic materials, complex processing conditions (i.e. clean room, specialized equipment), vacuum-coating steps, and elaborate encapsulation schemes is not as attractive as a polymer solar cell technology with lower performance that does not involve the disadvantages above. Further, an inferior technology may, in the end, be more useful if it can be produced using simple and existing techniques. As a part of this work, we detail and analyze the actual cost of the modules produced.

1.3. The matching of the product requirements to the capability of the product

Polymer solar cells currently provide efficiencies for laboratory cells that compete with amorphous silicon. In terms of operational stability and processing, however, the technology have so far been lagging significantly behind the inorganic semiconductor solar cells where processing in large volumes is established and the consumer is accustomed to a product with very long operational stability (lifetime). The inferiority of polymer solar cells based on the short operational stability and unexplored processing requirements should, however, not prohibit attempts to evaluate the technology in a real context as long as:

(1) the polymer solar cell performance meet the requirements of the application;
(2) the expectations of the consumer are met.

The efficiency that can be reached with polymer solar cells approach the 5–6% range for very small devices, but large area module efficiencies have so far been much lower. Further, the stability of solar cells has (in the cases where reported) been low, except for a few cases [15–22].

When choosing a subject for a first product it is important to ensure that the polymer solar cell can deliver enough energy for the application, even after having been subject to some degradation. This puts constraints on the choice of application. In realistic terms only relatively passive applications are suitable, i.e. audio applications. Light-emitting devices were for the purpose of this work deemed too power consuming and the choice fell on a small FM radio, that could be powered partially or in full by the polymer solar cells. In order to ensure as large as an active area as possible, without influencing the esthetics of the application, a hat was chosen. The solar cell device was placed on the top of the hat and the radio and ear plugs were integrated in the hat. The operational lifetime of the device was taken into account by directing the "Solar Hat" towards a music festival with a short duration of 1 week. It was deemed important not to let the consumer expect a longer operational period.

1.4. Motivation and aim of this work

This work is based on a recent report of a laboratory study of a polymer solar cell that exhibited a good operational stability in air [20,21]. Briefly, the device type offers a modest power conversion efficiency of ~0.2% under 1000 W m^{-2} at AM1.5G and up to 0.5% at lower light intensity 50–100 W m^{-2} at AM1.5G. More important, the entire processing is based on solution processing and does not necessarily include fullerenes. The only unsolved issue, vis-à-vis the aims described above, is that it employs indium tin oxide (ITO) as the transparent electrode. The aim of this work was thus to take the laboratory result and suitably modify it to a large-scale process. The device structure is shown in Fig. 1. From this
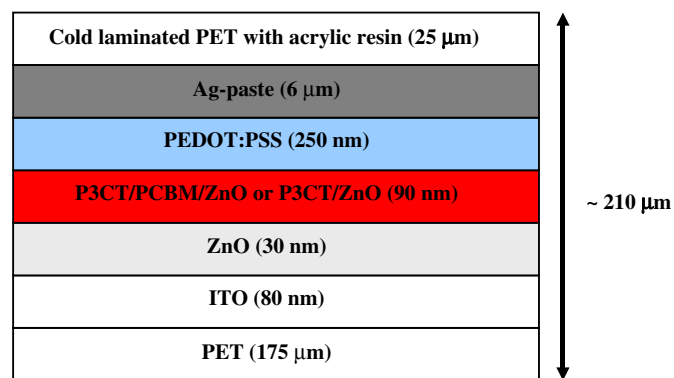

Fig. 1. The structure of the devices explored here. The thicknesses of the layers are not drawn to scale.

experiment, where many square meters of active solar cell area was printed, we demonstrated the processing speed, processing cost, the sacrifice in performance associated with going from laboratory cell to mass produced serially connected modules, materials consumption, statistics of module performance and application of the finished modules by public demonstration and free distribution.

2. Experimental

2.1. General materials

Poly-(3-(2-methylhexan-2-yl)-oxy-carbonyldithiophene) (P3MHOCT) was prepared on a large scale according to the literature [23]. The crude product was obtained by pouring the reaction mixture slowly into well-stirred methanol (10 volumes). It was then redissolved in toluene (50 mg mL^{-1}) and centrifuged at 2000 rpm for 30 min to remove a sludge-like material that contained metallic palladium nanoparticles (this step is vital). The palladium content of the crude product was analyzed according to the literature procedure and found to be >250 ppm [24–27]. Careful decantation and filtration through a 0.45 μm teflon filter, directly into vigorously stirred methanol (6 volumes), precipitated the product that was then filtered off and washed with methanol, and dried on a rotary evaporator at 50 °C. This gave a fluffy product that dissolved very rapidly in common solvents. No palladium was detectable in the final product using the azothioformamide test [25], and it was not necessary to purify the material further by treating with azothioformamide, while the batches used in the initial tests were purified thus. We ascribe the possibility for efficiently removing the palladium via centrifugation and filtering alone, to be due to the fortuitous interaction between the palladium nanoparticles and the polymer material in toluene (attempts to use other solvents such as chloroform and THF did not solve the problem). The total production gave 78 g of purified product. $M_n = 11,300$, $M_w = 36,900$, $M_p = 29,800$, PD = 3.3. WS-1 solvent was prepared according to the literature [28,29]. ZnO nanoparticles [30–33] were prepared according to the literature [20,21] on a large scale by mixing solutions of 59.4 g of Zn(OAc)$_2\cdot$2H$_2$O in 2500 mL of methanol and 30.2 g KOH dissolved in 1500 mL of methanol. The mixture was kept for 3 h at 60 °C, and during this period the particles started to precipitate. The dispersion was then allowed to stand without stirring at room temperature for 6 h allowing the particles to settle. The supernatant was decanted, followed by redispersion of the particles in 1000 mL of methanol. The particles were then allowed to settle for 12 h, decanted and

redissolved in 80 mL chlorobenzene to give 120 mL of a final ZnO solution with a concentration of 115 mg mL^{-1}. The yield of the ZnO varies considerably from batch to batch, and the typical range of ZnO concentration obtained is 90–250 mg mL^{-1}. The solution was used directly for obtaining the ink materials for the production of polymer solar cells by screen printing.

2.2. Preparation of the inks for printing

The inks for printing was prepared as close to use as possible, and were stored in air tight containers. The time between preparation and application in printing was 6 h for the P3MHOCT/ZnO (P3MHOCT/PCBM/ZnO) ink (PCBM = [6,6]-phenyl-C61-butyric acid methyl ester) and 26 h for the ZnO ink. While the inks were deemed quite stable and demonstrated to work even months after preparation, we chose to employ conditions that we could control to ensure reproducibility.

2.2.1. The ZnO ink

The ink for the transparent ZnO-based electron conductor (hole barrier, electron transport layer) was prepared by adding methoxyethoxyacetic acid (MEA) (1 g) to 200 mL of WS-1. A chlorobenzene–MeOH solution of zinc oxide nanoparticles (10 g nanoparticles ~87 mL of the 115 mg mL^{-1} solution) was mixed with MEA (1 g), and the two solutions were mixed with stirring. The initial turbidity quickly disappeared and the solution was evaporated at 70 °C for 30 min to remove most of the chloroben-

zene and methanol. A weight loss of 75 g was observed. The final volume of the solution was ~210 mL. The viscosity of the solution was 20.4 mPa s as measured at 24 °C at 30 s^{-1}. The printing of the ZnO ink is shown in Fig. 2.

2.2.2. The P3MHOCT/ZnO ink

The P3MHOCT/ZnO ink was prepared by dissolving P3MHOCT (5 g) in chlorobenzene (150 mL) and stirred at room temperature for 1 h. MEA (1 g) was added followed by WS-1 (200 mL). A ZnO (87 mL, 115 mg mL^{-1} solution containing 1 g MEA) was added, and the mixture was split in two equal parts. The first half was evaporated to a volume of 110 mL at 70 °C to remove most of the chlorobenzene. Care has to be taken to avoid precipitation at this point. If this happens a small volume of chlorobenzene can be added. The viscosity of the solution was 29.5 mPa s as measured at 24 °C at 30 s^{-1}.

2.2.3. The P3MHOCT/PCBM/ZnO ink

The P3MHOCT/PCBM/ZnO solution was prepared by taking the second part and adding 2.0 g PCBM dissolved in chlorobenzene (100 mL). The mixture was then evaporated to a volume of 110 mL at 70 °C to remove most of the chlorobenzene. The viscosity of the solution was 39.3 mPa s as measured at 24 °C at 30 s^{-1}.

2.2.4. The PEDOT:PSS and silver back electrode

The PEDOT:PSS (poly(3,4-ethylenedioxythiophene) poly(styrene-sulfonate)) layer was based on commercially available Orgacon EL-P
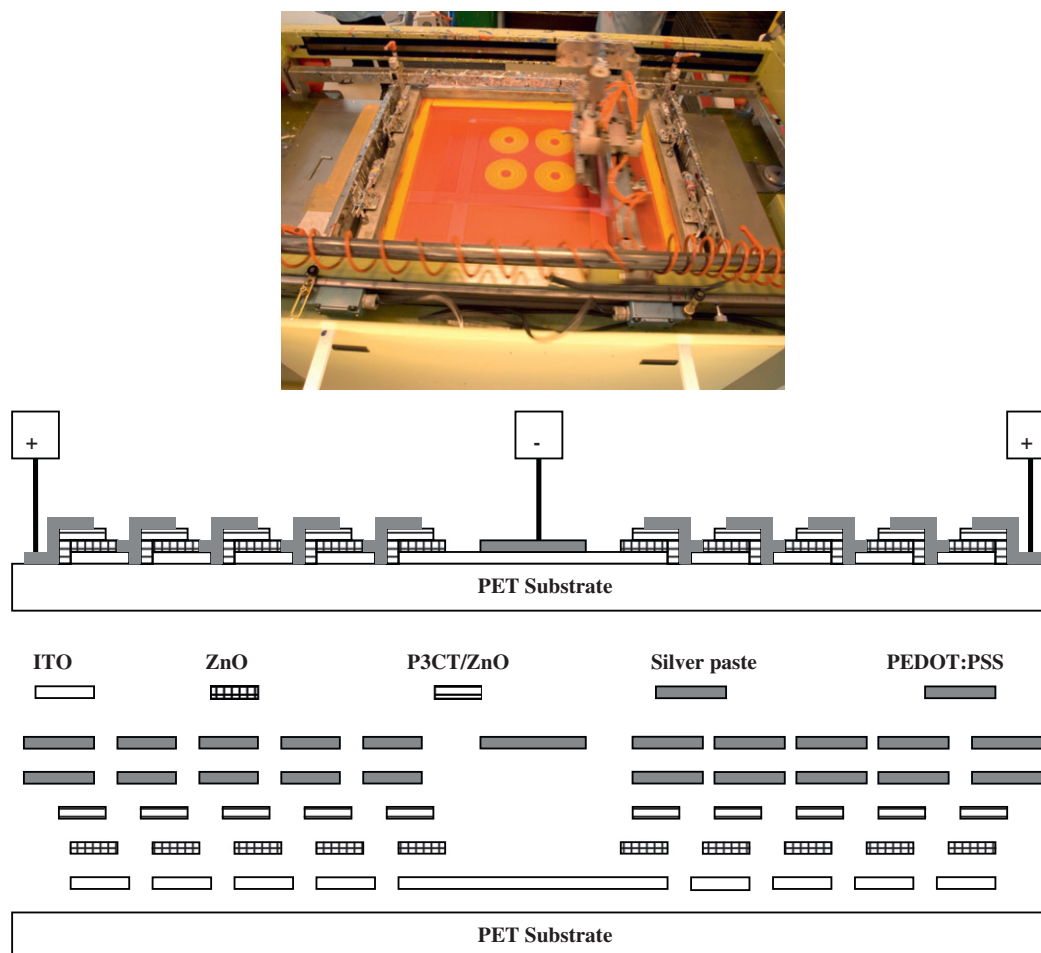

Fig. 2. Printing of the transparent ZnO nanoparticles solution which is visible as an opaque color (top). A schematic cross-section of the device is shown (middle) along with an exploded view of the layers (bottom).

5010 from Agfa and the silver electrode was based on silver migration-resistant thermosetting 5007 from Dupont. Both materials are designed for screen printing and were used as received.

2.3. Preparation of substrates

The substrates were prepared from ITO covered poly(ethylene terephthalate) (PET) (175 μm) rolls, having a roll width of 305 mm as received from Innovative Specialty Films (ISF, T-MOX). The nominal sheet resistance was $60\,\Omega\,square^{-1}$. The desired pattern was then printed, and the substrates were etched and stripped, entirely in a roll-to-roll (R2R) process. The roll was cut into sheets with four modules each. Holes were then locked for positioning during printing. It was found necessary to wash the substrates by immersion into 5% $NH_4OH(aq)$ in i-PrOH, followed by rubbing them using dust-free tissue, washing in pure i-PrOH, and finally drying using clean room tissue.

2.4. Preparation of devices

The area on the substrate was cleaned with a TekNek® roller immediately prior to printing to remove dust particles. During the preproduction runs this was found to significantly improve the number of working cells produced. The devices were prepared on the cleaned substrates by printing the ZnO/WS-1 solution through a 180 mesh screen. The printed sheets were collected in a rack and since the processing time extended for more than an hour this meant that the sheets that were printed first were left in the atmosphere as wet film for up to 90 min before entering the oven. After drying for 2 h at 140 °C and reposing at room temperature for 14 h, the ZnO films were insoluble and quite resistant to mechanical scratching. The subsequent layers were then printed. The P3MHOCT/PCBM/ZnO modules were printed as modules 1–1060, and the P3MHOCT/ZnO modules were printed as modules 1061–2124. The printing of each run took 45 min. and the cells were then put into the oven at 70 °C and ramped up to 140 °C. After drying and thermocleavage (P3MHOCT→P3CT, P3CT = poly-3-carboxydithiophene) at 140 °C for 4 h, the PEDOT:PSS (Orgacon EL-P-5010 from Agfa) was printed using a 165 mesh screen. This took 90 min. The modules were dried in the oven set at 120 °C. The temperature dropped to 90 and 120 °C was reached after 15 min. The modules were then left in the oven at 120 °C for another 10 min. Finally, Dupont 5007 silver migration-resistant screen printing ink was printed to complete the modules through a 120 mesh screen.

The silver prints were dried at 120 °C as follows: P3CT/PCBM/ZnO modules 1–524 were dried for 2 h, P3CT/PCBM/ZnO modules 525–1060 were dried for 30 min, P3CT/ZnO modules 1061–1636 were dried for 2 h, and finally, P3CT/ZnO modules 1637–2124 were dried for 30 min. The modules were then labeled, and every 10th sample was drawn for intermediate testing and was not laminated, but laser cut and crimped, to allow for establishing the effect of lamination. After lamination access to the individual cells in the module was not possible. Before laser cutting and crimping electrical contacts, the processed sheets, containing four complete modules, were cold laminated with a mechanical protecting layer. The lamination was carried out on top of the silver back electrodes, using a 25-μm-thick Fasson overlaminating polyester material from Avery Dennison, comprising a 270 mm wide PET film with a permanent acrylic-based adhesive. The overlaminating foil was narrower than the sheet, but wide enough to cover the individual modules. All the steps of the process, the materials consumption and the time required for each step is outlined in Fig. 3. The weight of the final modules including label and crimp connections was 4.6–4.7 g.
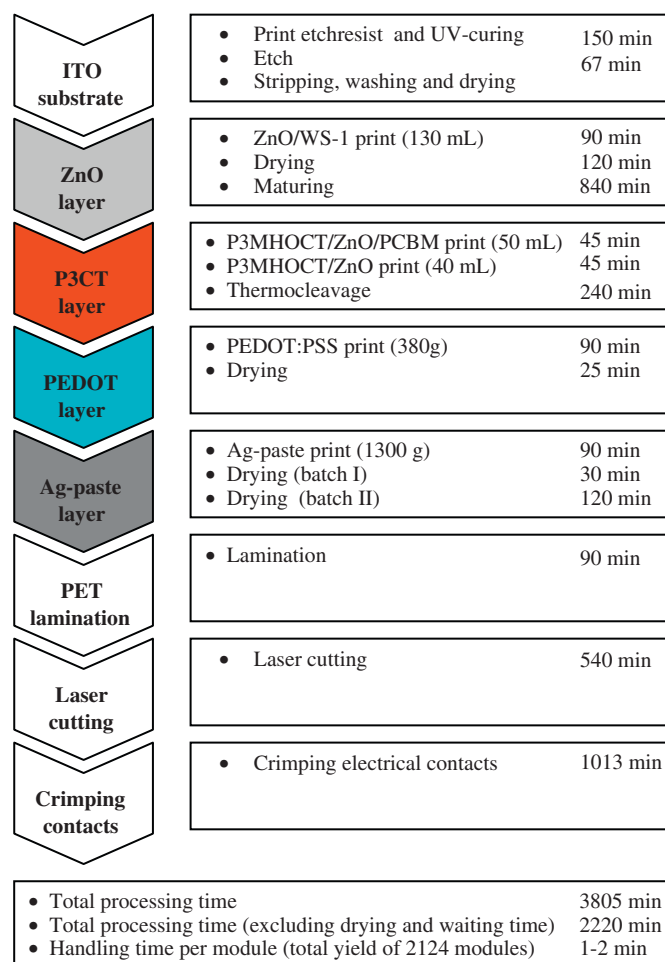

ITO substrate	• Print etchresist and UV-curing • Etch • Stripping, washing and drying	150 min 67 min
ZnO layer	• ZnO/WS-1 print (130 mL) • Drying • Maturing	90 min 120 min 840 min
P3CT layer	• P3MHOCT/ZnO/PCBM print (50 mL) • P3MHOCT/ZnO print (40 mL) • Thermocleavage	45 min 45 min 240 min
PEDOT layer	• PEDOT:PSS print (380g) • Drying	90 min 25 min
Ag-paste layer	• Ag-paste print (1300 g) • Drying (batch I) • Drying (batch II)	90 min 30 min 120 min
PET lamination	• Lamination	90 min
Laser cutting	• Laser cutting	540 min
Crimping contacts	• Crimping electrical contacts	1013 min

• Total processing time	3805 min
• Total processing time (excluding drying and waiting time)	2220 min
• Handling time per module (total yield of 2124 modules)	1-2 min

Fig. 3. A process flow chart outlining all the steps employed in this process along with the process time starting with 200 m of PET/ITO substrate that gave a final yield of 2124 completed modules.

2.5. Module testing

The production of solar cells was geographically remote with respect to Risø National Laboratory for Sustainable Energy, and a mobile test station was therefore devised so that the modules could be tested as they were produced. In order to be able to test the individual cells in the module a test jig was devised. The tester comprised a vacuum table with 6 concentric gold electrodes. To test a module it was simply placed on the vacuum table so that the printed circular electrodes matched the circular electrodes on the vacuum table. The individual cells in the module, their resistance, IV characteristics and that of the entire module were recorded. This setup proved to be particularly useful during the preproduction runs where measurements could be made on-site. The system was based on a Keithley 2400 and a Keithley 2700 with a Keithley 7705 switch matrix as described previously [34]. All the cells of the module were tested during the preproduction runs and every tenth module sheet was sampled during production. The setup was excellent for testing device resistance and photovoltaic function using an ambient light source. Since these devices change significantly in performance during the first few days after production full characterization was not meaningful at this stage, and this setup was used only as a quality assurance tool to discard modules that were not functioning properly. All the modules from the final production were tested later under simulated sunlight with KHS 575 solar simulators

from Steuernagel Lichttechnik operating at $1000\,W\,m^{-2}$, AM1.5G, $45 \pm 5\%$ relative humidity, $72 \pm 3\,°C$. The high humidity levels are typical for a Danish summer time (the humidity may reach as high as 60–65% indoor during rainfall but this was not experienced during our experiments). The spectrum of the solar simulator was checked using an optical spectrum analyzer calibrated for measuring irradiance. The incident light intensity of the solar simulator was calibrated bolometrically using a precision spectral pyranometer from Eppley Laboratories (www.eppleylab.com). The incident light intensity was monitored continuously during measurements using a CM4 high-temperature pyranometer from Kipp & Zonen (www.kippzonen.com). The lifetime measurements were performed using part of a setup described earlier [34] where up to 7 devices can be studied per solar simulator. The modules were connected and taped flat onto a glass surface and measurements were carried out in the ambient atmosphere, $1000\,W\,m^{-2}$, AM1.5G, $45 \pm 5\%$ relative humidity, $72 \pm 3\,°C$. Six cells were tested in each run; three cells from the 1–1060 batch (two laminated and one sample cell) and three cells from the 1061–2124 batch (two laminated and one sample cell). The effect on the curing time for the Dupont 5007, the effect of lamination and the effect of adding PCBM on module stability was established in this manner.

3. Results and discussion

3.1. Choice of polymer solar cell technology

The choice of polymer technology was made on the basis of the prerequisites that; the device preparation should be possible in the ambient atmosphere, existing printing equipment should be used, the final modules should be stable during storage in the ambient atmosphere, no vacuum-coating steps should be necessary and the final modules should have an operational stability allowing for public demonstration. The only solar cell technology presented so far that is reasonably stable in the ambient atmosphere, without encapsulation, is based on ZnO nanoparticles and P3CT. The first report on this device type employed processing in a glovebox due to the sensitivity to humidity of ZnO nanoparticles prepared by the method of Wormelsdorf et al. [30–32] when redispersed in an organic solvent such as chlorobenzene. This problem was overcome by stabilising the ZnO nanoparticles with the carboxylic acid MEA [21].

3.2. Choice of printing method

Screen printing, as a technique for creating a 2-dimensional pattern, date back to the beginning of the 20th century and has been touted as the most versatile of all printing techniques. It is simple, fast and reproducible. Furthermore, the requirements for its use are very modest and it can in essence be carried out anywhere in the world with little prerequisites. It is attractive to pursue the idea of printing all the layers of the solar cell using this technique alone, but it poses some challenge as screen printing, in contrast to most other printing techniques, gives a very large wet thickness of the printed film. This is especially problematic for the active layers where good control of the film thickness and morphology is required. A complication is the exposure of the ink to the atmosphere during printing. One particular problem in this respect is that the ink must not dry out on the mask and an open time of several hours is required for an industrial process. If volatile solvents are used they dry up in the screen printing mask and thus deteriorate the definition of the printed pattern. The use of screen printing has been reported for the formation of the active layer in polymer solar cells in a few cases [12,13,35,36].

3.3. Making the solar cell technology compatible with screen printing on flexible substrates

The critical requirement of a long open time of the ink on the screen printing mask and the problem of a large wet thickness of the print, in relation to polymer solar cells that rely on a thin active layer film, were solved through the development of thermocleavable solvents and fillers [28,29]. These new materials allow for a near infinite open time of the ink since they do not evaporate and dry out at room temperature. Secondly, the thermocleavable solvents are of a reasonably high viscosity giving a stable print, even at high dilution of the solutes and upon thermocleavage. By removal of the thermocleavable solvent thin active layers can thus be prepared. This allowed for preparing and printing inks for the transparent ZnO layer and for the active layer. The remaining layers were easily realised using screen printing. The ITO layer was prepared by printing a UV-curable etch resist followed by etching and stripping in a complete roll-to-roll process. The PEDOT:PSS and the silver electrodes were screen printed using commercially available screen printing inks, respectively, Orgacon EL-P 5010 from Agfa and silver migration-resistant 5007 from Dupont. One final limitation was the curing time of the ZnO and the active layer. In the case of ZnO the printed layer had to be dried at $140\,°C$ for 2 h followed by interaction with the atmosphere for 14 h to obtain insolubility. For the active layer 4 h at $140\,°C$ was required to thermocleave P3MHOCT to P3CT, in an extent that was sufficient to convey insolubility. The temperature stability of the PET substrate is the most significant limitation to this approach. Thermocleavable materials currently have a cleavage temperature of around $200\,°C$ in the best cases. Thermocleavage of P3MHOCT to P3CT does take place at lower temperatures, but the time required for completeness of the thermocleavage reaction increases.

3.4. Choice of printed pattern

In order to take advantage of the possibility of 2-dimensional patterning that screen printing gives access to, and to accommodate the available geometric area in the application, a circular module outline was chosen. The solar cell module was designed to be integrated in a "Solar Hat" at the very top of the hat, which most easily, is a circular area. The advantage of using the top surface of a hat as the platform for the solar cell is that there is a reasonable guarantee that the solar cell surface is exposed to sunlight when available. In order to achieve a reasonable module voltage, and to minimize sheet-resistive losses, the module was chosen as a serial connection of individual solar cells shaped as concentric rings (shown as a side view in Fig. 2 and as the printed active layer in Fig. 4). The requirement in a serially connected module for an equal current being produced by the individual cells implies that the active area of the individual cells must be identical, and this again implies that the outermost rings are much thinner than the innermost rings. The device module was chosen to comprise five such solar cell rings. Each ring had an active area of $15\,cm^2$ giving a total active area of $75\,cm^2$. The outer diameter of the module was 130 mm and the total area of the module was thus $133\,cm^2$. The geometric fill factor is thus 56% with a corresponding aperture loss of 44%. In order to minimize the sheet-resistive losses the outermost contact was chosen as the printed silver electrode. In the case of Dupont 5007, printed through a 120 mesh screen and cured at $120\,°C$ for 2 h, the typical sheet resistance was $<1\,\Omega\,square^{-1}$, whereas the ITO had a typical sheet resistance of $70–90\,\Omega\,square^{-1}$ after patterning, etching, stripping and cleaning. In this manner, the innermost circle had the ITO as the point of current extraction. By printing silver in the

Fig. 4. A wet print of the active layer that is very even when freshly printed, while some shadowing due to the poor quality of the underlying ZnO layer is evident (top left). A magnification of the rings for the final module showing unevenness of the red polymer layer due to dewetting during drying and thermocleavage of the active layer printed on the uneven ZnO layer (top right). An extreme case of reproduction of the mesh structure in the final print at a magnification of 60 (bottom left). A slightly uneven print without the mesh structure at a magnification of 60 (bottom right). (For interpretation of the references to color in this figure legend, the reader is referred to the web version of this article.)

central part the conduction paths in ITO were essentially limited to the active area.

3.5. Preproduction considerations and processing of entire modules using screen printing

The transfer of the single laboratory cell to industrial processing on a large scale was achieved in several necessary steps. First, a fully screen printed cell was prepared in the laboratory and optimized on the actual module pattern. An automated laboratory screen printer was employed for this purpose. The optimization involved the modification of inks and the rational choice of screen printing mesh, tension and orientation of the mesh fibers to obtain an optimal print. A commonly observed problem with screen printing is that the mesh structure is reproduced in the final print (see Fig. 4). A series of problems pertaining to the effect of drying on the quality of the transparent ZnO barrier layer was also solved. The wetablility of the ZnO layer by the active layer ink

during drying and thermocleavage was severely affected in some cases (see Fig. 4). These problems were effectively solved, and a process where single modules could be printed on a laboratory scale was devised. The next step involved preproduction runs where the same procedure and inks were used under the same industrial conditions as intended for the final production. While this may seem to be a trivial task, it proved necessary to perform three preproduction runs before it was possible to reproduce the laboratory experiments under industrial conditions. In the three preproduction runs 116 (7–9 April 2008), 136 (5–7 May 2008) and 272 modules (15–17 May 2008) were prepared, respectively. The optimized conditions were then employed in the final production run where a total of 2124 cells were produced (9–11 June 2008) at Mekoprint Electronics A/S.

3.5.1. The transparent conductor

The substrate material was purchased as 175-μm-thick PET with a sputter-coated overlayer of ITO. The nominal sheet

resistivity as supplied was $60\,\Omega\,\text{square}^{-1}$. The substrate was processed in roll lengths of 200 m and a width of 305 mm. The motif in each print comprised the transparent electrode pattern for four modules and was printed using a UV-curable etch resist. The motif was printed on a R2R coating line from Klemm comprising: unwinder, edge alignment, corona treater, dust remover, screen printer, inspection table, UV-curing station, four ovens, inspection section and winder. The total printing time was 150 min. The ITO was subsequently etched using a full R2R etching machine comprising etching baths ($CuCl_2$), stripping baths (NaOH), washing baths (demineralized water) and drying section (hot air). The total etching, stripping washing and drying time took 67 min. The roll with the transparent electrode pattern was then aligned, cut into sheets (305×310 mm) and alignment holes were punched, making it ready for the manual screen printer. The substrates were subsequently cleaned by immersion in isopropanol containing 5% aqueous ammonia for 20 min followed by washing in pure isopropanol, rubbing with dust-free paper wetted with isopropanol and finally drying in air. The washing procedure was the most time consuming as it was done manually and required 3 people for 240 min (it is likely that this process can be automated). A total of 537 sheets were obtained. The practical yield of 83% compared to the theoretical yield of 645 sheets is due to adjustment in each of the processes and discarding of poor sections. The ITO is not error free and often sections of the ITO simply delaminate during the process described here.

3.5.2. The electron-transporting layer

The ZnO nanoparticle solution in WS-1 was printed on a manual screen printer using a 180 mesh screen. The loss during adjustment of the screen with respect to the etched ITO pattern was 6 sheets (24 modules). Since it is possible to contact directly through an Ag–ZnO–ITO stack we made experiments with a non-patterned ZnO layer, however, it proved very difficult to print such a large area without getting thickness variation in the print. It was an advantage to have a thin screen emulsion line between the rings that enabled the screen to detach from the sheet during printing giving an even layer. Further, a weak point in the current design is that the ZnO layer does not form a strong bond to ITO and delamination upon flexing of the final module was observed at the ITO–ZnO interface. This was solved by avoiding ZnO at the edge and at the center. A good attachment of the silver paste directly to ITO/PET was thus ensured (see Fig. 2). The substrates were printed through a 180 mesh screen and it was found necessary to clean the surface with a TekNek® roller immediately prior to printing. This delayed the manual process somewhat and it took 90 min to print all 537 sheets. The total consumption of ZnO printing ink was 130 mL. The substrates were placed on racks and were dried in an oven with a total capacity of 600 sheets. The TekNek® roller efficiently removed dust particles and possibly part of the exposed interface. The cleaning pads employed for each printing run were analyzed using time-of-flight secondary ion mass spectrometry (TOF-SIMS) [37] to establish which impurities that are observed in the production environment (described in section 3.6.). It was further possible to establish which impurities that were observed after each print (vide supra).

3.5.3. The active layer

The active layer was printed using a 180 mesh screen. The ink for the active layer comprised either a mixture of P3MHOCT and ZnO nanoparticles in WS-1 or P3MHOCT, PCBM and ZnO nanoparticles in WS-1. It was found that a small amount of residual chlorobenzene 2–5% was beneficial for the film-forming process. There was in this case no loss during adjustment and alignment of the screen with respect to the etched ITO/ZnO pattern, as the 6 sheets that were used for adjustment during printing the ZnO layer could be used again (24 modules). The printed active layer was heated in an oven for 4 h at 140 °C, which was sufficient to impart insolubility that is required during the printing of the ensuing layers. A total of 1060 modules of P3CT/PCBM/ZnO modules were prepared using a total ink volume of 50 mL in 45 min, and 1064 P3CT/ZnO modules were prepared using a total ink volume of 40 mL in 45 min. A TekNek® Roller was used to clean the surface immediately before each print and the adhesive cleaning paper was analyzed using TOF-SIMS (vide supra).

3.5.4. The hole conductor

Several different PEDOT:PSS screen printing formulations were tested in preproduction (Orgacon EL-P 3000, 4000 and 5000 series from Agfa and Baytron S V3 from H.C. Starck, now Clevios). The Orgacon EL-P 5010 was found experimentally to perform best and was used in the production run. All the modules were printed using a 165 mesh screen, and the entire printing procedure was completed in 90 min. A TekNek® Roller was again used to clean the surface immediately before each print and the adhesive cleaning paper was analyzed using TOF-SIMS (vide supra). The PEDOT:PSS print was dried in an oven for 10 min at 120 °C once the temperature had been reached. When entering two racks into the hot oven the temperature dropped to 90 °C and increased to 120 °C in 15 min.

3.5.5. The back electrode

The silver electrode was printed using silver migration-resistant Dupont 5007 through a 120 mesh screen. The entire printing procedure took 90 min and a TekNek® Roller was used to clean the surface immediately before each print and the adhesive cleaning paper was analyzed using TOF-SIMS (vide supra). The final modules were dried in the oven at 130 °C and the two batches, respectively P3CT/PCBM/ZnO and P3CT/ZnO, were each split in two groups and dried for two different lengths of time, 30 and 120 min. The two different drying times were employed to explore the advantages of longer drying times which increases the conductivity and adhesion of the silver electrodes. It was, however, found that the longer drying times led to poorer performance and therefore it would seem that one should strive for the shortest possible curing time.

3.5.6. Drawing samples, labeling, laminating and crimping of contacts

The complete modules were back-laminated using simple 25 μm PET film with an acrylic-based adhesive allowing for cold lamination. After lamination it is not possible to access the individual cells in the module. In order to carefully analyze the effects of the later processing steps (laser cutting and crimping) all modules were labeled manually with an individual serial number, including knowledge of when they were printed, which of the four positions they had on the printed sheets and where they were positioned in the oven. The sheets were in identical positions during all four printing cycles. After labeling, every tenth sheet was drawn as a sample and characterised using the setup. All modules (excluding the samples) were then cold laminated. This took a total of 90 min. All the cells (including the samples) were laser cut to a diameter of 130 mm after lamination. The laser cutting system has the disadvantage that it is slower than cutting with a knife tool. But it has the advantage that it is readily adaptable to a small series of modules as is the case here. It may further have the advantage that the back lamination and the PET substrate are efficiently welded together. The laser cutting operation was lengthy and could only be performed at about

Fig. 5. The final modules comprising screen printed layers, back lamination and crimped contacts (left) and all the 2124 modules (right).

150 modules per hour, requiring a total of 14 h for completion. The final step was the crimping of contacts, which was made by manual crimping through both contacts. The crimping was the most time-consuming step and required about 27 s per connection (54 s per module). This step should either be avoided in a high volume product or made fully automated. It is likely that a connector system that efficiently allows for contacting to the final cell will be required to reduce the cost of the use of the modules. The current circular design, however, does not make this possible without extra printing steps and a different topology should probably be sought. If the circular design was mandatory it would be possible to print an insulating UV-curable epoxy on top of the silver electrodes, followed by printing a silver pattern, allowing for extraction of the current from the central contact in the design to the edge of the module. This procedure is commonly employed in flexible multilayer printed circuits and would not present a challenge, but would require two extra printing steps. The additional cost of this would be minor as seen in the cost analysis for these modules (*vide supra*), where the materials and substrate carry the majority of the cost for the completed modules shown in Fig. 5.

The final modules were then analyzed and characterised and all the data used for statistical analysis of the yield.

3.6. TOF-SIMS analysis of the TekNek® cleaning pad

The use of a roller from TekNek® was found to have a significant impact on the number of working cells produced. The substrates were roller cleaned immediately prior to printing to remove dust particles. In order to avoid accumulation of dust particles on the roller and possible reattachment of the dust particles on the substrate, a TekNek® cleaning pad was used to clean the roller. The cleaning pad consists of a sheet of foil with an adhesive surface that attaches the dust particles when the roller is applied, i.e. the pad removes the dust particles from the roller. One roller is used for the whole production, i.e. cleans all the substrates. However, a fresh sheet of cleaning pad was used prior to printing of the individual layers. In summary, prior to printing the ZnO layer, the ITO surface/substrate was roller cleaned and the roller was subsequently cleaned using the cleaning pad. After having printed the ZnO on all of the substrates the cleaning pad was saved for analysis. Prior to printing the P3CT:ZnO layer the ZnO surface/substrate was roller cleaned and the roller was

cleaned using a fresh cleaning pad that was saved for analysis, etc. In this way four used cleaning pads were saved each with accumulated dust particles for the printing of one particular layer.

In order to investigate whether the roller removes more than just dust particles the surface of the cleaning pads were analyzed using TOF-SIMS [37]. TOF-SIMS provides chemical surface characterization in the form of surface mass spectral data. With this technique it is possible to determine whether the roller removes "chemistry" from the substrates, i.e. material that is not visible using a microscope, as is dust particles. It is of interest to explore whether the roller removes unavoidable chemical contamination from the substrate and, more importantly, whether this contamination ends up on the cleaning pad or whether it, via the roller, is transferred to the other substrate types. It is furthermore of interest to explore whether the printed layer material is, via the roller, transferred to the next layer. It is of vital importance that material from one surface/substrate is not transferred to the surface/substrate of another layer. The surfaces/substrates constitute the interfaces in the resulting solar cells, which is where the highly important charge transfer processes take place, that are highly sensitive towards contamination.

By choosing more or less unique mass spectral markers in the TOF-SIMS analysis, it is possible to distinguish material on the surface of the cleaning pad. To obtain the more or less unique mass spectral markers a piece of solar cell was analyzed using TOF-SIMS imaging. This particular solar cell had misaligned printed layers, and the layer of silver paste was missing. This enabled TOF-SIMS characterization of the resulting exposed layers. Fig. 6A shows an optical image of a selected part ($1 \times 0.4\,cm^2$) of the misaligned layers, and Fig. 6C shows a schematic of a cross-section of the misaligned layers. The eye in Fig. 6C indicates the point of view in the optical image. TOF-SIMS can create a chemical image of a surface (i.e. TOF-SIMS imaging) with a probe depth (i.e. information depth) of only 1 nm. This means that only the outer surface is detectable. Fig. 6B shows a combined TOF-SIMS image over the exact same area as the optical image.

A unique mass spectral marker is chosen such that the ion intensity distribution is only visible in one particular layer. The ion image in Fig. 6B consists of the ion intensity distributions of $C_2H_5O^+$ (marker for PEDOT:PSS), CHO_2^- (marker for P3CT:ZnO), and Zn^+ (marker for ZnO). The ITO surface was not exposed in this part of the solar cell, however, this does not matter since In^+ can be regarded as an obvious unique marker for ITO. A pristine cleaning
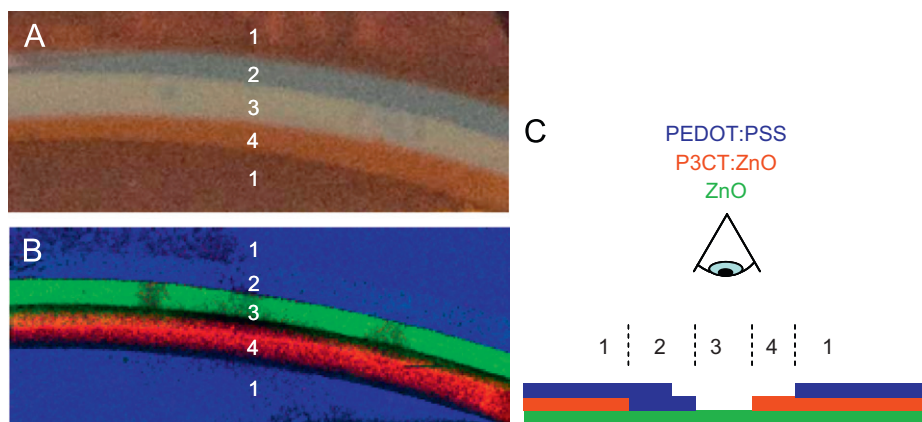
Fig. 6. (A) Optical image of a $1 \times 0.4\,\mathrm{cm}^2$ area of a solar cell without the Ag layer and with misaligned layers of ZnO, P3CT:ZnO and PEDOT:PSS. (B) Combined TOF-SIMS ion images (normalized with respect to the intensity) of the exact same area using $C_2H_5O^+$ as a marker for PEDOT:PSS, CHO_2^- as a marker for P3CT:ZnO, and Zn^+ as a marker for ZnO. (C) Schematic cross-section of the misaligned layers (not drawn to scale). The eye represents the point of view of image A and B. The numbers corresponds to the numbers in A and B.

pad was analyzed as a reference such that the cleaning pad background could be disregarded. The information obtained so far is sufficient to analyze the cleaning pad surfaces. However, the TOF-SIMS ion images revealed additional information regarding contamination of the solar cell surface. The entire surface analyzed contains silicone contamination (not shown). However, considering the probe depth and since other species are visible (e.g. solar cell material) it must be a sub-monolayer of silicone.

It is not (directly) possible to quantify species on the surface. Sodium contamination is mainly observed on the PEDOS:PSS layer surface (not shown). Potassium is almost exclusively observed on the ZnO layer surface (not shown). Potassium hydroxide was used in the preparation of the ZnO nano particles, which explains the presence on the ZnO surface. In fact, potassium is observed on the surface corresponding to 3 and 2 in Fig. 6, which suggests that potassium has migrated through the PEDOT.PSS layer to the surface of the PEDOT:PSS layer. Several other typical contaminants were observed on the solar cell surface. However, these additional observations do not provide vital information so they will not be discussed. The cleaning pads were analyzed using optical imaging and TOF-SIMS imaging. Fig. 7A shows an optical image of a pristine cleaning pad surface. The surface appears to be homogeneous. Fig. 7B shows a used cleaning pad after having cleaned the roller that cleaned the ITO surface. There are clearly large particles and fibers on the pad surface, so it is thus possible to conclude that the roller removes particles and fibers from the ITO surface. The used cleaning pad surface appears to be inhomogeneous as expected. Fig. 7C is a TOF-SIMS ion image showing the In^+ intensity distribution on the used cleaning pad surface corresponding to Fig. 7B. Flakes and particles of ITO appear to have been removed from the ITO surface. This fact should not constitute a problem if only a minor part of the ITO layer is removed, e.g. if only loose flakes and particles are removed. Fig. 7D shows the intensity distribution of $Si_2C_5H_{15}O^+$, which is a marker for silicone (or silicone-like species). The mass spectrum (not shown) of the pristine cleaning pad surface is similar to the mass spectrum (not shown) of silicone rubber. If silicone rubber (or something similar to that) is present in the cleaning pad material, then one would expect silicone oligomers to be present in the material and especially on the surface of the cleaning pad. This could possibly explain the presence of silicone contamination evenly distributed on the solar cell surface (not shown). So using the roller will possibly contaminate all the surfaces with silicone. The impact of silicone contamination on the solar cell performance is not known. However, considering the apparent low level

of silicone contamination (sub-monolayer) it is not considered to be a vital problem.

TOF-SIMS mass spectra were acquired from each cleaning pad surface. Mass spectral markers for the species that were present on the used pad, but not on the pristine pad, were selected together with species that were also present on the pristine pad, but elevated in intensity. The fact that all surfaces are cleaning pad surfaces (i.e. the same) enables semi-quantitative information to be extracted with respect to the contamination. It is possible to compare the relative concentration of a particular contaminant between pads, but it is not possible to compare different contaminants, not even on the same pad. Fig. 8 shows the semi-quantitative results of the TOF-SIMS spectrometry analysis of the cleaning pad surfaces. Surface I–V corresponds to:

- Surface I: Pristine cleaning pad
- Surface II: Cleaning pad from cleaning of ITO surface
- Surface III: Cleaning pad from cleaning of ZnO surface
- Surface IV: Cleaning pad from cleaning of P3CT:ZnO surface
- Surface V: Cleaning pad from cleaning of PEDOT:PSS surface

There are several interesting observations in Fig. 8. For example, Fig. 8I shows the relative content of silicone on the cleaning pad surfaces. The pristine pad surface (I) has a higher content of silicone compared to the used pads (II–V) that have practically the same silicone content. This observation suggests that the previously mentioned silicone oligomers, which tends to surface segregate, is being used up on the cleaning pad surface by being transferred to the solar cell substrates/layers via the roller. The fact that silicone is still detected on the used pads is due to the time it took from production to analysis of the pads. The silicone oligomers had time partly to segregate from the bulk to the surface. Another very positive result is the one in Fig. 8H that shows, what is already known from Fig. 7C, that ITO is partly removed from the ITO surface. However, the interesting part is that indium is only observed on Surface II, i.e. there is no transfer of ITO to the other solar cell layers/substrates. In fact, none of the printed layers have been transferred, via the roller, to other layers, which must be regarded as a very positive result. Most of the remaining contaminants (Figs. 8A–G) were detected as atomic ions, which are all very easy to detect in the mass spectrum. Low levels of possible organic contamination is difficult to detect under these circumstances especially if they produce fragment ions (produced by the ionization process of the analysis) that are
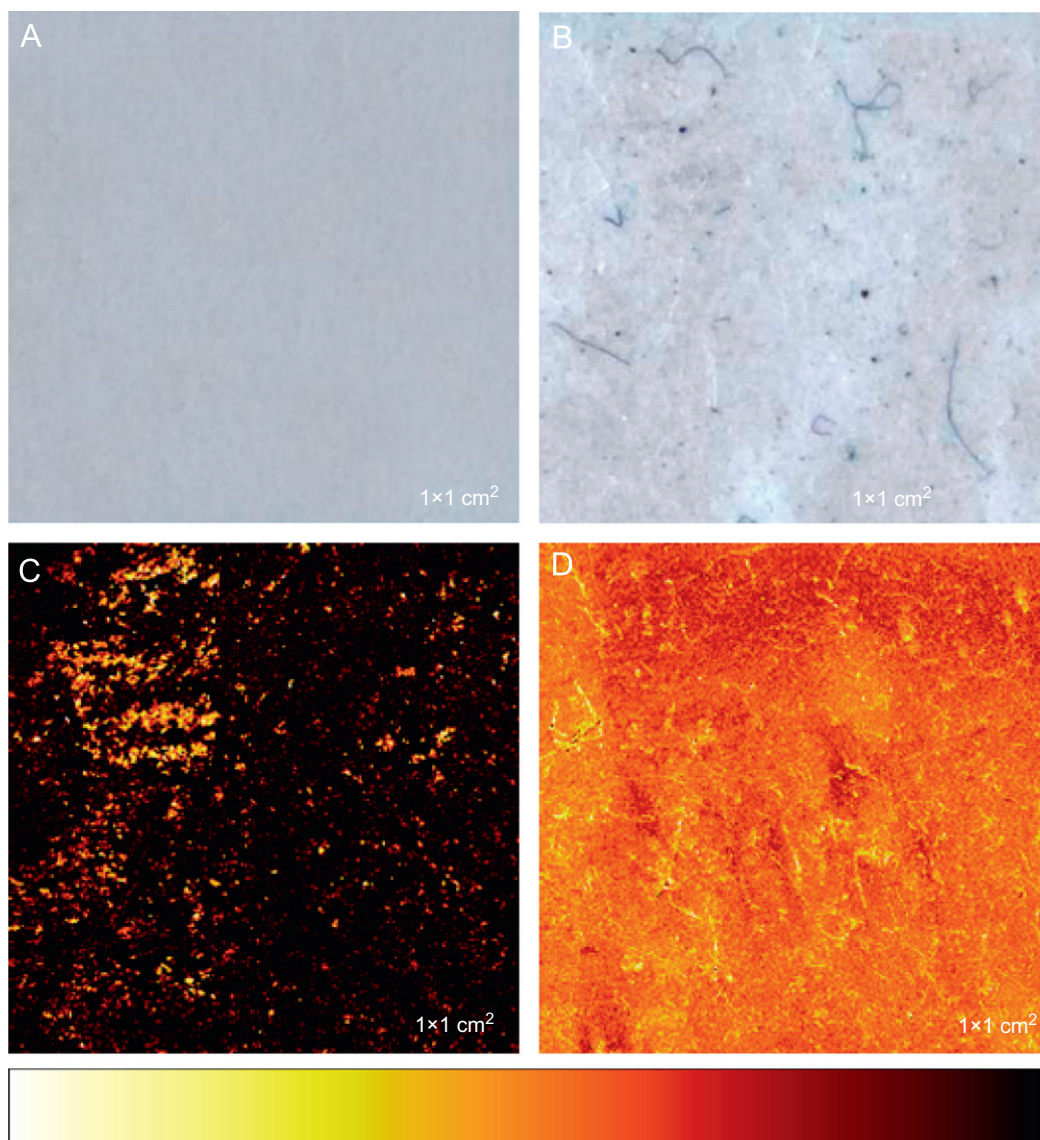
Fig. 7. (A) Optical image of a pristine cleaning pad surface. (B) Optical image of a cleaning pad that was used to clean the roller that cleaned the ITO surface. (C) TOF-SIMS ion image (normalized with respect to the intensity) showing the In^+ intensity distribution over the exact same area as in B. The intensity bar at the bottom refers to C and D only. (D) TOF-SIMS ion image (normalized with respect to the intensity) showing the $Si_2C_5H_{15}O^+$ (silicone marker) intensity distribution over the exact same area as in B.

the same as the one generated from the cleaning pad material or has the same organic contamination as the cleaning pad material (the chemical composition of the cleaning pad material is unknown). There appears to be a trend for most of the remaining contaminants shown in Fig. 8. Surface II has the highest contents of contamination, which then shows a more or less steady decrease when going to Surfaces III, IV, and V. The observation appears to be systematic, which suggests that the roller starts out by being "very" contaminated with these species, either from the ITO surface or from the roller it self. The roller then gets steadily cleaner as it is used on subsequent substrates and cleaning pads. These contaminants are presumably present in a very low level. It is uncertain to what extent they interfere with the solar cell processes.

In summary, according to the TOF-SIMS analysis results of the cleaning pad surfaces and on a solar cell surface the following conclusions can be made. Part of the ITO material is removed by the roller and ends up on the cleaning pad. The printing materials were not detected on the cleaning pads. ITO and the printing materials are not transferred, via the roller, to other printing

layers. Silicone is believed to be present on the cleaning pad surface that efficiently gets transferred, via the roller, to the subsequent printing substrates as a more or less evenly distributed sub-monolayer. Common surface contaminants (Mg, Al, Ca, K, F, Cl, S_xO_y) are present on the roller during the initial cleaning step, which either originates from the roller itself or from the ITO surface. The presences of these contaminants are then steadily decreased in the subsequent printing of other materials, i.e. the contaminants are transferred, via the roller, to the surfaces of the other printing materials. It is unknown to what extent the observed spreading of contamination (as a result of using the roller) has on the solar cell performance. However, it seems that the benefit of using the roller outweighs possible degrading effects caused by the spreading of contamination.

3.7. Performance of the modules

One noteworthy aspect of the modules produced is that the performance, that is reached, (Fig. 9) is significantly lower than
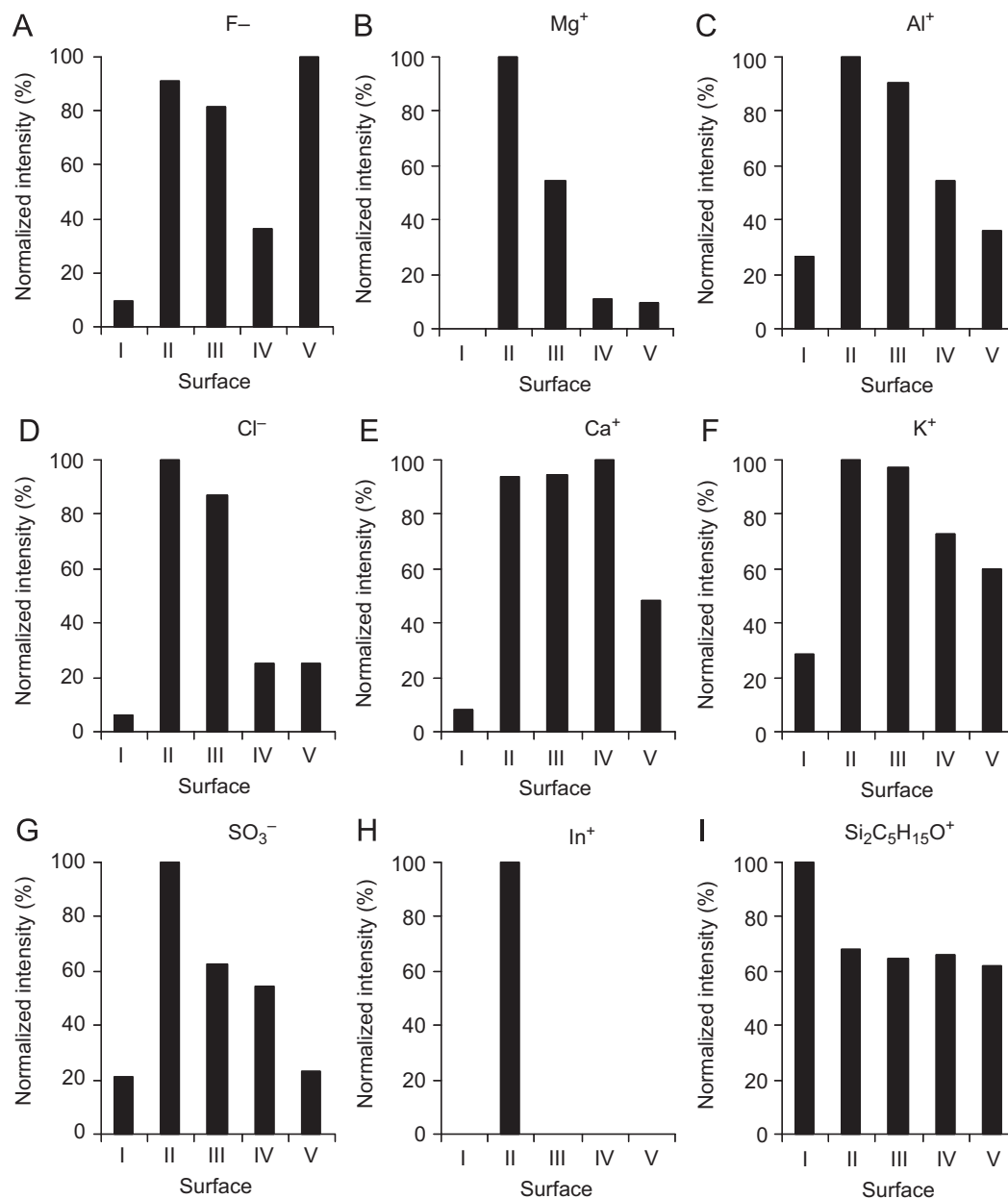
Fig. 8. Semi-quantitative TOF-SIMS results obtained on cleaning pad surfaces. Five different surface locations were analyzed on each sample surface and the average value was used. Each signal was normalized against the total ion intensity and thereafter normalized such that the highest value in a series (I–V) corresponds to 100%. Surface I: Pristine cleaning pad, Surface II: Cleaning pad from cleaning of ITO surface, Surface III: Cleaning pad from cleaning of ZnO surface, Surface IV: Cleaning pad from cleaning of P3CT:ZnO surface and Surface V: Cleaning pad from cleaning of PEDOT:PSS surface.

the performance for the model devices prepared in the laboratory [20,21]. While difficult to rationalize, the decrease in performance by a factor of 20 for the best cells and a factor of 25–30 for the average cell, some points can be highlighted. The model devices were of small active area (1 cm^2) and prepared on rigid glass substrates with high conductivity ITO (5–8 Ω square^{-1}) using spin-coated ZnO, P3MHOCT/ZnO and PEDOT:PSS. On the other hand, modules prepared during production were prepared on flexible substrates bearing an inferior quality of ITO that was subject to etching beforehand, and an in comparison relatively poor cleaning procedure. The devices were of larger area (by a factor of 15) and comprised 5 serially connected cells in a complex geometry. All the layers were prepared by the same printing technique, and there were necessarily some sacrifices due to the ink used for film formation, the film formation and the handling

procedure (long waiting times before drying, slow heating due to the large heat capacity of the racks and materials, lower degree of cleanliness in the production environment, etc.). Some of the disadvantages could perhaps be resolved by improving the production method, and ideally it is anticipated that one could approach the laboratory result by a much smaller margin. The rule of thumb for inorganic semiconductor-based cells is that the industrially produced modules yield about 60–70% of the performance obtained for lab-scale devices [38]. One clear correlation between the process parameters and the performance was the curing time for the silver back electrode, which would seem to indicate that the shorter the curing time the better. Curing times of 30 and 120 min were employed here and the short curing time was significantly better. In the laboratory cells shorter curing times of 3–15 min have been employed, and it would in
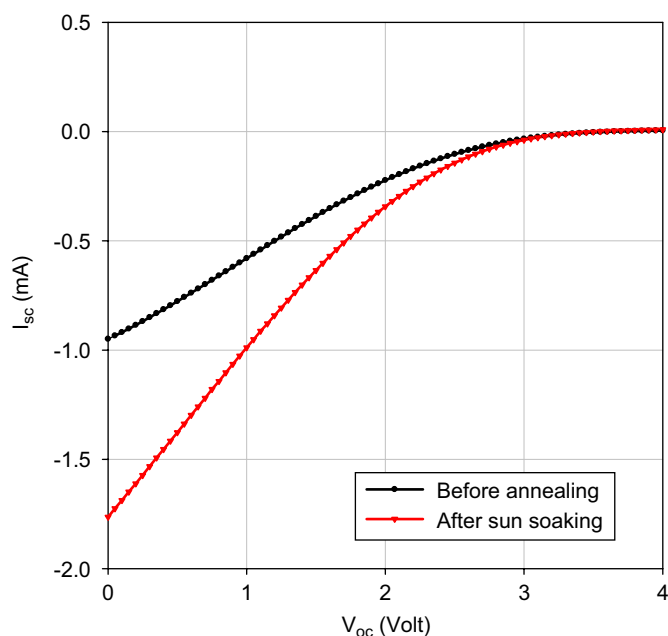
Fig. 9. Typical *IV* curve for one of the good modules. Module number 1836 from the final production run is shown. The module was a P3CT/ZnO device where the silver electrode was cured for 30 min. The devices improve upon illumination. The initial *IV* curve is shown along with the performance after sun soaking for 10 min (1000 W m^{-2}, AM1.5G, $72\pm2\,^\circ$C, $40\pm5\%$ relative humidity). After sun soaking: $V_{oc} = 3.53$ V, $I_{sc} = -1.76$ mA, FF $= 0.16$; MPP $= 1.01$ mW (1.17 V/-0.86 mA).

Fig. 10. I_{sc} (mA) (open circles) and V_{oc} (V) (closed circles) data for all the 2124 modules produced.

future optimization be worthwhile to shorten the curing time. With the current method it is not possible to reduce the curing time much below 30 min due to the thermal latency of the system (racks, cells, oven, etc.), but one possibility would be to use the R2R Klemm line, where a curing time of 4 min should be possible. The current Klemm line has four stretches of near vertical hot air ovens with a total oven length of 20 m.

With the current ink formulations vertical drying is, however, not possible due to running of the ink upon heating before final drying (due to a viscosity drop of WS-1 at high temperature [29]). Since the silver is printed last we could not offer a solution for this with the current method, while many clear advantages would be achievable by using the R2R Klemm line for printing and processing all the layers of the modules.

3.7.1. Data for the final 2124 modules

Before the final production some preproduction runs were carried out. In the first preproduction run most of the cells produced were not working. Out of 116 modules only two of the printed modules had all five cells in the series connection working. The reasons for the failure for most of the individual cells were short circuits. We further analyzed the number of working cells as a function of where the module was printed on the sheet. Out of the four positions one of them did not produce one single functional cell, whereas the other three positions produced functional cells, and the two functional modules were both from the corner opposite the one with no functional cells. We linked this to the adjustment of the screen and the firmness of attachment to the vacuum table. We further found that cleaning would be desirable to obtain a better quality of the print. In the second preproduction run we employed a better cleaning procedure, that involved aqueous ammonia as a volatile base, to aid in removal of etch resist that had not been stripped after patterning of the ITO. Further removal of dust particles and loose material was employed immediately prior to printing using a
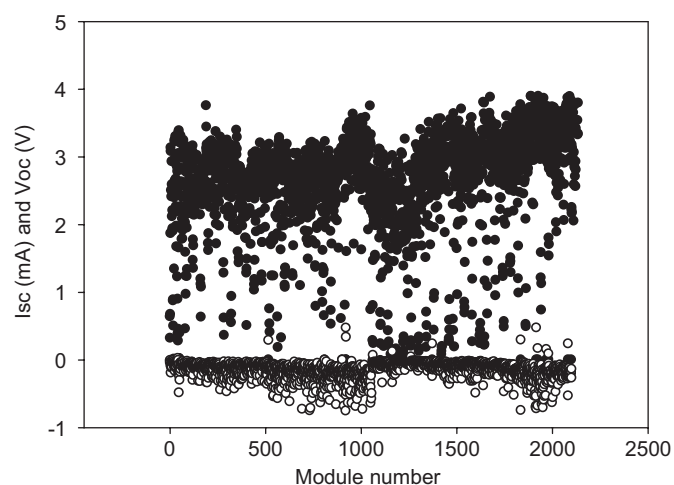
TekNek® cleaning roller. This improved the number of functional modules produced, and out of the 136 modules produced 92 were completely functional. During production *IV* curves were measured on every tenth module—that is on every 10th sheet having four modules. This happened just after curing of the backside silver electrode, but before lamination etc. All the individual solar cell rings were therefore exposed and individual *IV* curves for each cell as well as an *IV* curve for the module could be measured and parameters extracted. Since this preliminary characterization happened during production at the factory floor it was not feasible to employ a solar simulator, but a conventional lamp was used (60®W Incandescent reflector lamp, OSRAM CONCENTRA-TA© SPOT R63). A test stand with a circular array of gold-plated ring-type contacts were devised. Overall measurement time for each module was about 1 min. The data were only used to qualitatively test if the cells and module were functional.

Accurate performance measurements using simulated sunlight were performed after lamination, laser cutting and crimping of the modules 10 days post-production. As shown in Fig. 10, it is clear that the short circuit current for modules improve significantly towards the end of the production run. The P3CT/PCBM/ZnO modules (module numbers 1–1060) and the P3CT/ZnO modules (module numbers 1061–2124) were much better at the end of the run. Further, when plotting the product of the I_{sc} and the V_{oc} for the modules it was found that there was a significant difference with the curing time employed for the back electrode (Fig. 11). Module numbers 1–524 and 1061–1636 were cured for 2 h and module numbers 525–1060 and 1637–2124 was cured for 30 min.

It is quite likely that the improvement towards the end of the run is linked to the waiting time between printing and drying of the ZnO layer and of the P3MHOCT/ZnO or P3MHOCT/PCBM/ZnO layer.

While the ZnO nanoparticles had been stabilized with MEA, it is possible that interaction with humidity from the atmosphere during the resting time on the drying racks resulted in this effect. The resting time should be kept shorter. Another possibility is the effect of the age of the ink on the screen during printing. The quality of the print and the film may improve with the age of the ink. The module performance shown in Figs. 9–12 are recorded for pristine modules 10 days post-production. The performance was found to improve by a factor of 2–3, mainly due to an increase in the current upon soaking in the Sun for 10 min. It was, however, not feasible to sun soak all the modules and record the data again.

When viewing the performance in the figures a significantly larger stable performance should be anticipated. The good modules produced in excess of 1 mW when illuminated at $1000\,W\,m^{-2}$, meaning that the power conversion efficiency for the active area ($75\,cm^2$) is around 0.013%, or around 15–20 times poorer then the laboratory modules [20,21]. Upon examination of the perfor-

mance of all the modules by making a scatter plot of V_{oc} versus I_{sc}, as shown in Fig. 12, the typical behavior and the variation in module performance is clearly visible. Some qualitative observations can be made that are consistent with the laboratory experiments and they are that the addition of PCBM leads to a small increase in the current but also a lowering of the voltage. Further, the curing time for the silver electrode has a significant influence on the performance and the shape of IV curve, which would seem to indicate that transport limitations are present in the device [39]. This could be due to oxidation at the surface of the silver particles in the back electrode. From the scatter plot in Fig. 12 it is evident that most of the modules concentrate at $I_{sc} \approx -0.1$ mA and $V_{oc} \approx 3$ V. A tail of modules with higher values of I_{sc} exists up to ca. -0.8 mA. Upon annealing of the devices it is anticipated that the devices will improve in current by a factor of 2–4, and that the voltage will stay roughly constant. One reassuring point was that the final production run had few problems with short-circuited modules and the majority of the modules (>90%) had voltages in the 2–4 V range.

3.7.2. Comparison with earlier work

The performance of the modules prepared here offer some improvement in performance as compared to earlier reports where the active layer was screen printed onto flexible substrates and the area was large [12,13]. The processing speed for the ITO and the active layer in these prior cases was similar to this report, but the remaining part of the processing was slow. There have also been reports of large area devices on rigid substrates with power conversion efficiencies on the order of 2% [46,47], both from this
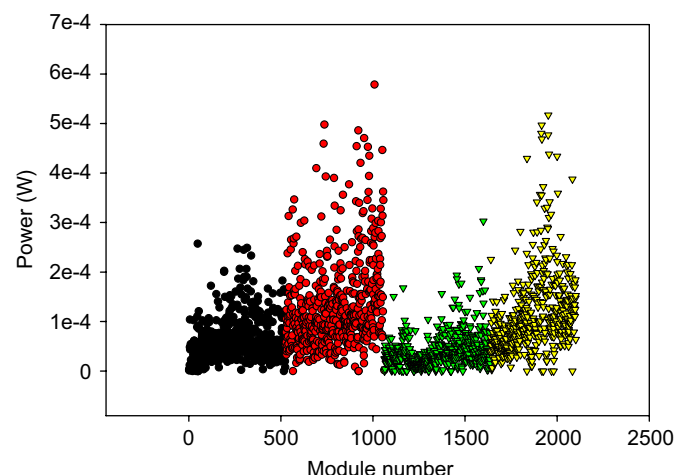

Fig. 11. Plot of $I_{sc} \times V_{oc}$ (power) for each of the four series of modules black spheres: PCBM/2 h curing, red spheres: PCBM/0.5 h curing, green triangles: ZnO/2 h curing, yellow triangles: ZnO/0.5 h curing. (For interpretation of the references to color in this figure legend, the reader is referred to the web version of this article.)
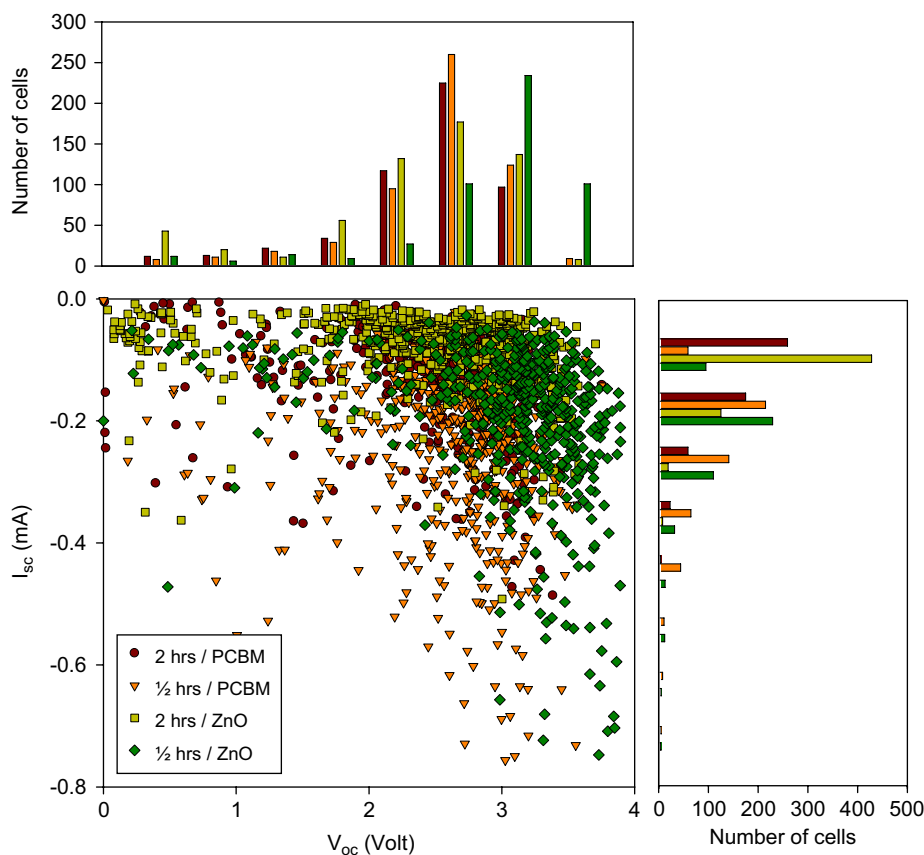

Fig. 12. Scatter plot of V_{oc} versus I_{sc} (middle) with each marker denoting a single module. The plots on each side show the number of modules in discrete intervals (0.5 V for V_{oc} and 0.1 mA for I_{sc}). Four different categories of modules are labeled individually. Those containing PCBM in the active layer are brown spheres (2 h curing time for the silver paste) or orange triangles (0.5 h curing time for the silver paste). Two other categories with ZnO as the only acceptor are shown as light green squares (2 h curing) and green diamonds (0.5 h curing). (For interpretation of the references to color in this figure legend, the reader is referred to the web version of this article.)

laboratory and from others. It should, however, be stressed that the total processing time for these individual modules is measured in days and in the case of the modules prepared here the processing time is measured in seconds (*vide supra*).

3.8. Stability considerations

Devices based on P3CT and ZnO are quite resilient towards both oxygen and water under illumination and has been ascribed earlier [19,20] to several factors. The stability towards water is due to the inverted nature of the device such that the metallic electrode chosen is inherently less reactive. The stability towards oxygen has been ascribed to the electron-withdrawing nature of the carboxylic acid moieties that lower the position of the electronic levels while keeping the band gap roughly constant. The electronic energy levels for P3CT and carboxylated thiophenes have been reported to be lowered by about 0.4–0.5 eV, depending on processing and annealing conditions [23,48]. Finally, it has been suggested that P3CT has a very poor ability to sensitize singlet oxygen [20]. The overall observations regarding stability that can be made based on the devices prepared in this production are that:

(1) The process of lamination seems to be beneficial for the devices (no special oxygen/water barriers involved).
(2) The initial performance is significantly lower than the performance obtained during stable operation.
(3) The stable performance is quickly reached during illumination.
(4) Thermal annealing of the cells post-production is not beneficial.
(5) The good modules generally exhibited good operational stability under illumination and the modules that were poor in the beginning failed quickly.

The modules were tested for operational stability in the as-produced form under ambient conditions by connecting the modules using alligator clips to the crimped connections. Devices were tested in the ambient atmosphere under simulated sunlight ($1000\,W\,m^{-2}$, AM1.5G, $72\pm2\,°C$, $45\pm5\%$ relative humidity). The storability of the produced modules was good and they were produced 1 month in advance to the demonstration. The
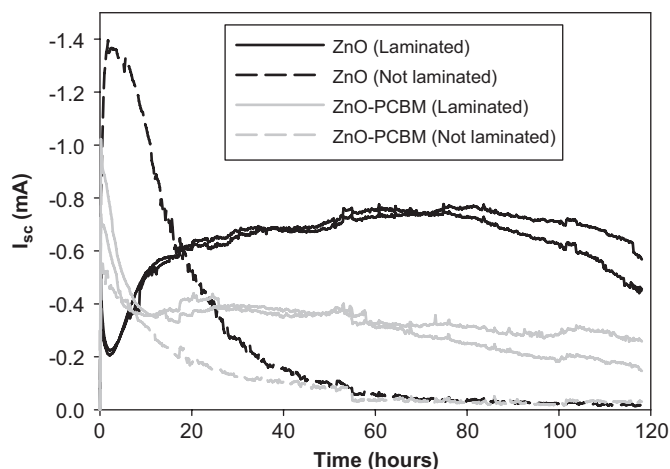

Fig. 13. A comparison of the short circuit current as measured every 10 min for complete modules cured for 30 min after the final Dupont 5007 print. The non-laminated devices quickly degrade in performance. Measurements on encapsulated devices were carried out in duplicate and exhibit very similar behavior for both P3CT/ZnO and P3CT/PCBM/ZnO modules. In all cases the devices without PCBM were the best-performing over time.

functional modules from the preproduction runs that had been kept under ambient conditions with the relative exclusion of light performed as well as initially after more than 3 months. Fig. 13 shows the qualitative differences in stability between P3CT/PCBM/ZnO and P3CT/ZnO where it is clear that the modules without PCBM perform better and are more stable. While the PCBM modules have a slightly higher initial value for the current it quickly drops, whereas the modules without PCBM exhibit improvement of the current for a significant period of time before degradation sets in. This is consistent with earlier findings [20,21]. One possible explanation of the observations, that the devices perform better after some illumination time (that includes UV-light), is the interaction between ZnO and molecular oxygen under UV-illumination. It has been suggested that molecular oxygen binds to the surface of the ZnO particles in the dark and creates a trap for electrons in the conduction band of ZnO. Illumination with UV-light leads to desorption of molecular oxygen and removal of the traps [49]. The lamination on the back electrode for mechanical protection using 25-µm-thick PET with an acrylic adhesive has an estimated oxygen transmission rate (OTR) and water vapor transmission rate (WVTR) of $\sim130\,cm^3\,m^{-2}\,day^{-1}$ and $15\,g\,m^{-2}\,day^{-1}$, respectively [40,41], and is expected to perform as a mechanical barrier only. The effect on the stability is, however, evident as shown in Fig. 13 where a comparison between modules that had been laminated and some of the modules sampled during production that had not been laminated.

The laminated modules exhibit good stability. Finally, the effect of the curing time of the silver back electrode was examined and it was found that the shorter curing time gave rise to better stability and a better performance.

3.9. Cost analysis, breakdown of production time and possible routes to improvements

The cost analysis of polymer solar cells is very complex, and depending on the purpose of the analysis many different conclusions can perhaps be arrived at. We have chosen to break down the cost of the modules produced here into the materials consumed, the time involved and the actual cost to us in €module^{-1}. From the data we present it should be possible to rationalize what the materials consumption and the cost of similar technologies will be using the scale and method employed here. It should also be evident how to proceed if wishing to reduce the production and materials cost.

3.9.1. Cost of P3MHOCT, PCBM and ZnO

The active layer in the most efficient polymer solar cells made to this date rely on a mixture of a fullerene derivative and a synthetic conjugated polymer material. The fullerene component act as an electron acceptor and electron conductor and while these materials are available on a large scale they can still be identified as a component that will make up a considerable part of the total cell cost. The polymer material is the electron donor and hole conductor, and while most materials employed today are as costly as the fullerene component, there is a good possibility that this cost can be reduced through optimization. A device is further comprised of a carrier substrate, barrier layers and electrodes, where one is preferably transparent. For this study we prepared the materials for the printing ink on a large scale and detailed the cost in terms of materials (as obtained from Aldrich as the chemical supplier) and in terms of the man power involved in synthesis and preparation. For the devices that involve PCBM we used the cost as obtained from Solenne BV. PCBM has a cost of $100\,€\,g^{-1}$ when purchasing on the scale of 100 g. The synthesis of P3MHOCT involves five synthetic steps starting from a commercially
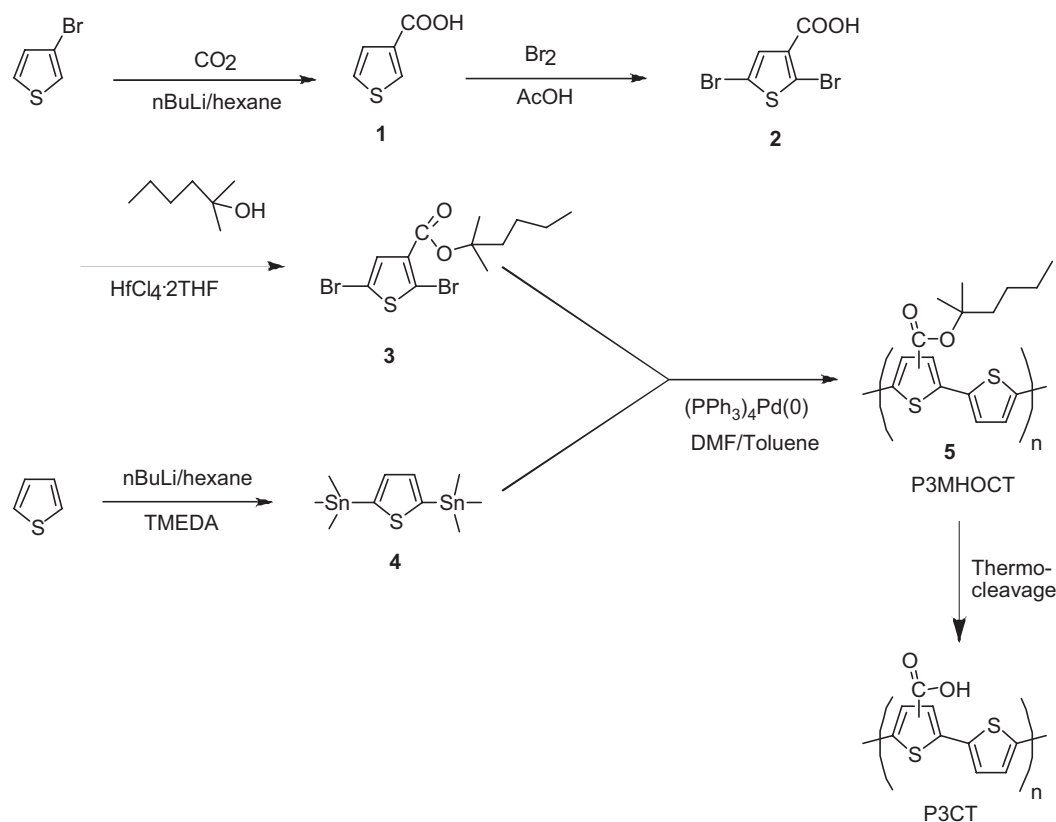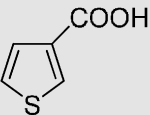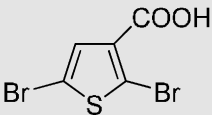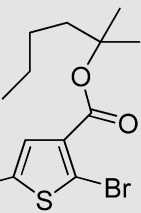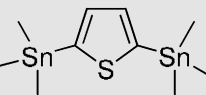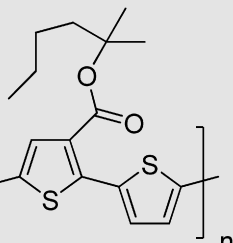
Fig. 14. Synthetic procedure to P3MHOCT and thermocleavage to P3CT. The materials consumption is given in Table 1.

Table 1
Cost analysis of P3MHOCT based on a reasonable synthetic scale.

Compound	1	2	3	4	5
No of runs	7	4	6	5	6
Total materials	3-Bromothiophene (160 g)	Compound **1** (100 g)	Compound **2** (200 g)	Thiophene (40 g)	Compound **3** (105 g)
	n-BuLi (1.6 M) (0.7 L)	Br$_2$ (100 mL)	2-Methyl-2-hexanol (100 mL)	Trimethyltinchloride (180 g)	Compound **4** (112 g)
	Hexane (1.5 L)	AcOH (1 L)	HfCl$_4$·2THF (10 g)	TMEDA (140 mL)	Palladium cat. (22 g)[a]
	Dry THF (100 mL)		CH$_2$Cl$_2$ (2 L)	nBuLi (1.6 M) (600 mL)	Dry toluene (3 L)
			DMAP (100 g)	Silica (2.5 kg)	Dry DMF (500 mL)
			DIC (100 g)		Methanol (50 L)
			Silica (2.5 kg)		Filters (50 pcs.)
			Heptane (10 L)		
			EtOAc (1 L)		
Yield (g)	100	200	105	112	78
Materials cost per step (€)[b]	700	42	1155	850	1260
Man hours per step[c]	35	8	70	35	150
Materials cost per gram (€ g^{-1})[d]	7	0.21	11	7.6	16.1
Total cost per gram (€ g^{-1})					357

THF = tetrahydrofurane, DMAP = 4-dimethylaminopyridine, DIC = diisopropylcarbodiimide, TMEDA = tetramethylethylenediamine, DMF = dimethylformamide.
 [a] The palladium catalyst was Pd(PPh$_3$)$_4$ and was prepared from PdCl$_2$, triphenyl phosphine using hydrazine as reducing agent at a cost 15 € g^{-1}.
 [b] The materials cost is based on the price as ordered from Aldrich.
 [c] The cost for man hours was based on Danish rate for a lab technician 80 € h^{-1}.
 [d] The material cost excludes the cost of the material from the previous step.

Table 2
Cost analysis of ZnO nanoparticles preparations and WS-1.

Material	ZnO (MEA) nanoparticles	WS-1
No of runs	2	–
Total materials	$Zn(OAc)_2.2H_2O$ (120 g)	–
	KOH (60 g)	
	Methanol (10 L)	
	Chlorobenzene (160 mL)	
Yield	27.6 g	1.5 kg
Materials cost $(€)^a$	104.9	3180
Man hours[b]	2	150
Cost per gram $(€\,g^{-1})^c$	9.6	10

[a] The materials cost is based on the price as ordered from Aldrich.
[b] The cost for man hours was based on Danish rate for a lab technician $80\,€\,h-1$.
[c] The weight is based on ZnO nanoparticles. A total of 240 mL of $115\,mg\,mL^{-1}$ was obtained.

available starting material (3-bromothiophene) as outlined in Fig. 14. We chose to prepare P3MHOCT on a medium scale and obtained after purification 78 g of the material. Based on the consumption of materials and man power we calculate a cost of $357\,€\,g^{-1}$ for this material as detailed in Table 1.

The zinc oxide nanoparticles are, in comparison to PCBM, a very low-cost acceptor material with a cost as prepared for this work of $9.6\,€\,g^{-1}$.

The zinc oxide nanoparticles are employed in two of the layers constituting the final module; the transparent electron transport layer and the active layer. A very important material for preparing printable inks is the thermocleavable solvent WS-1 [28,29], which makes up a significant amount of the total ink cost due to the large amounts required. WS-1 was prepared at a cost of $10\,€\,g^{-1}$ and the cost of zinc oxide solution and WS-1 are summarized in Table 2. Three ink formulations were employed; the ZnO nanoparticle ink for the transparent electron conductor in WS-1, P3MHOCT/ZnO for the active layer in WS-1 and P3MHOCT/PCBM/ZnO in WS-1. The cost for these three ink formulations were 10.5, 19.4, $21.4\,€\,g^{-1}$, respectively. Based on the consumed materials during production the cost of the individual layers are obtained as: $0.64\,€\,module^{-1}$ for the transparent ZnO layer, $0.73\,€\,module^{-1}$ for the transparent P3MHOCT/ZnO layer and $1.01\,€\,module^{-1}$ for the transparent P3MHOCT/PCBM/ZnO layer.

From this it is clear that the cost of the ink makes up a large part of the final module cost. Some of the cost could perhaps be reduced by avoiding the use of an expensive synthetic solvent but even if this is eliminated the cost of the active material is significant and simpler and lower cost materials should be developed.

3.9.2. Cost of ITO, PET and ITO on PET

The transparent conductor in most reported polymer photo-voltaic's is generally based on indium-tin-oxide as this is a very high-performing transparent conducting oxide (TCO). Further, ITO has fortuitously advantageous electronic interactions with con-jugated organic materials through well-positioned electronic energy levels. The problem with indium, however, is that it is a highly costly and scarce element. The cost of indium increased more then 10-fold from year 2002–2005 and has been stable since then at about $450–600\,€\,kg^{-1}$. There have been very little effort so far dedicated to replace indium in transparent conductors and the few convincing solutions that exist rely on silver, PEDOT:PSS or composites thereof [42–44]. By contrast PET, which is employed as the substrate material, is of quite low cost and while it exists in many qualities the requirements as a substrate for organic photovoltaic's are not cost limiting. The requirements are a good optical transparency and thermal stabilization allowing for

processing of thin films at elevated temperatures without excessive shrinkage and deformation of the film. The bulk cost of bottle-grade PET is currently around $55\,€\,ton^{-1}$. One square meter of the PET-ITO substrate employed in this study is thus mostly PET by weight with a thickness of $175\,\mu m$ implying a weight of $\sim260\,g\,m^{-2}$ for the PET film and ITO with a thickness of $\sim80\,nm$ giving a weight of $0.57\,g\,m^{-2}$ ($\sim0.47\,g$ indium). The raw material cost of $1\,m^2$ of PET-ITO is $0.21–0.28\,€\,m^{-2}$ in terms of ITO and only $0.014\,€\,m^{-2}$ in terms of PET. The processing costs for the PET-ITO are high and involve sputtering in vacuum and the commercial cost of the PET-ITO employed are significantly higher than the raw materials cost, while these should apply in the high volume approximation. The cost of the ITO on PET in the volume employed in this study was $36\,€\,m^{-2}$. Since we discard approxi-mately half of the area during processing due to spacing between the modules, and we have some loss in the process this gives us a loss of 54% and a grand total of PET-ITO cost of $1.03\,€\,module^{-1}$. The overlaminating foil has a cost of $2.64\,€\,m^{-2}$ and including loss this implies a materials cost for the lamination of $0.073\,€\,module^{-1}$.

3.9.3. Cost of PEDOT:PSS and silver back electrode

The Orgacon EL-P 5010 has a cost of $837\,€\,kg^{-1}$ when purchased in small quantities (2 kg). The material is a thick paste with a viscosity of $50,000\,mPa\,s$ and quite a lot of paste is required on the screen printing mesh to ensure filling of the mesh after each print. We recovered the material that had not been used after the printing run and our consumption of 380 g for the entire production is the gross loss in the PEDOT:PSS container after the run. The cost of PEDOT:PSS is thus $0.15\,€\,module^{-1}$. The silver back electrode is also a relatively thick paste with a nominal viscosity of 20,000–$40,000\,mPa\,s$ that was purchased at a price of $520\,€\,kg^{-1}$. The total consumption was 1300 g of material, which is equivalent to $0.32\,€\,module^{-1}$. Since the sheet resistance of the printed silver electrode was $<1\,\Omega\,square^{-1}$ and the ITO is significantly higher, it is likely that some cost reduction could be achieved by decreasing the printed silver electrode thickness thus increasing the sheet resistance without compromising the performance.

3.9.4. Overall cost of the modules produced

Based on the cost of the materials and the amount of man and machine hours spent, it is possible to work out a cost of the modules covering all expenses. This has been outlined in Table 3.

Table 3
Module cost analysis for polymer solar cells as produced in this study divided into materials cost, process cost and total module cost

Material	Process cost $(€\,module^{-1})^{a,b}$	Materials cost $(€\,module^{-1})$	Step cost $(€\,module^{-1})$
PET-ITO	0.287	1.03	1.317
ZnO layer	0.056	0.64	0.696
P3MHOCT/ZnO	0.056	0.73	0.786
P3MHOCT/PCBM/ZnO	0.056	1.01	1.066
PEDOT:PSS	0.056	0.15	0.206
Ag paste	0.056	0.32	0.376
Lamination	0.056	0.073	0.129
Laser cutting	0.339	–	0.339
Crimping contacts[c]	0.636	0.053	0.689
Total[d]	1.542	2.996 (3.276)	4.538 (4.818)

The total number of solar cell modules was 2124 modules with and individual area of $133\,cm^2$.
[a] The process cost is based on a flat rate of $80\,€\,h^{-1}$ that includes man power and machine time.
[b] The drying times and repository times have been excluded from the calculation.
[c] Based on 2 gold-plated crimp connections per module.
[d] The cost for the P3MHOCT/ZnO active layer is given and the cost of P3MHOCT/PCBM/ZnO active layer is given in brackets.

The total cost implies that the modules could be produced and supplied without loss. Due to the poor performance of the modules it is not meaningful to work out a cost of electricity in $\in W^{-1}$, but as noted earlier [20] this technology outperforms small batteries at the laboratory level when taking the entire life span of the product into account. In this case where the general module performance is significantly lower than the performance reached my laboratory cells, the technology barely compete with a small battery and the cost is significantly higher. It is natural to conclude that a higher performance would improve the value for this type of solar cell. While we have no immediate solution to the much poorer performance as compared to lab cells, a meaningful exercise is to analyze the cost and identify the cost-limiting materials and processes as these can be assumed general.

It should be underlined that the cost analysis in Table 3 is based on the cost of production in Denmark, and that it would be possible to reduce these costs by exploring man power in countries where the cost is lower. When examining the process cost it is clear that laser cutting and crimping contacts involves handling of the individual module and this should be avoided. By using a knife tool the cutting of the devices can be performed at the same speed and cost as the screen printing or lamination cycles ($0.056 \in$ module^{-1}). Further, the use of crimped contacts should be discouraged and printed contacts should be supplied with the module instead. This would reduce the total process cost to $0.68 \in$ module^{-1} where the ITO processing now makes up a significant (42%) of the processing cost. A printable electrode would be highly desirable and is a subject worthy of study. These devices were prepared on a 305 mm roll width in sheet dimensions of 305×310 mm and with the equipment available in this study it would have been possible to process in larger area, thus increasing the speed and lowering the process cost. With the Klemm R2R line available it would be possible to use a 610 mm roll width, and a quadrupling of the number of printed modules per hour would be possible without altering the layout. A small improvement could also be reached through organizing the modules a little better on the substrate thus optimizing the printed area per total roll area. A vast improvement would also be possible if the Klemm line could be used for printing all the layers. Currently only the ITO layer is fully R2R processed. The current modules had a total process time of 81 s module^{-1} including drying (i.e. total processing time per module). Most of the process time is drying time and from this point of view the printing processes are already efficient and not rate limiting. By excluding the drying time, which in essence does not require labor, and by exclusion of laser cutting and crimping, since these steps are too costly to be of practical use, the modules prepared here required 26 s module^{-1}. This number for the processing time can be used to estimate the gain obtained by going to full R2R processing of all layers employing a roll width of 610 mm. In such a case the processing time would decrease to 11 s module^{-1}. The reason for the relatively small decrease is that the washing and etching time does not change using the current method. It should be kept in mind that the process cost for the method presented here are a small proportion of the total module cost and the materials cost are the dominant cost factor that should be sought reduced first.

It is clear that ITO makes up a large proportion of the materials cost as does the active layers. The PEDOT:PSS and the silver electrodes are relatively low-cost factors for the current modules. The screen printing solvent WS-1 is part of the reason that these materials costs are so high. With the current printing method and device presented here there is little room for improving the materials cost. The best solution that can be offered is that the addition of PCBM is avoided, that a thinner silver electrode layer is employed and that crimping contacts are avoided. This would bring the overall materials cost down to $2.77 \in$ module^{-1}. An improved cost for the modules produced here would present knife cut and crimp free devices and would have a potential cost of $3.45 \in$ module^{-1}. This is a significant improvement as compared to the actual value of $4.53 \in$ module^{-1} quoted in Table 3. What would be required is, however, a much larger reduction in cost and this would have to be sought through a replacement of ITO with a printable transparent conductor, and possibly the use of a different printing technique for the ZnO and the P3MHOCT/ZnO layers that employ low-cost solvents. Finally, it would be advantageous to find a polymer material that was lower in cost than P3MHOCT by a factor of at least 10.

3.10. Application of the modules at the Roskilde festival 2008 in Denmark

Having demonstrated that functional molecules could be produced in a convincingly large number, where the largest proportion ($>90\%$) gave more than 2 V in V_{oc}, which was required to charge the battery in the application with a FM radio, many small electronic gadgets (FM radio, Soduko game, pulse measuring device, pocket calculator, clock, etc.) were considered, of which some were more suited then others. Our intention was to distribute 1000–2000 "Solar Hats" with the polymer solar cell powering an FM radio as the Roskilde Festival is a music festival [45]. The polymer solar cell technology chosen had the potential to fully power the radio with an active area of 75 cm^2 and more importantly it had an operational stability in air and a shelf life that should grant a reasonable chance of success in the application.

The modules we produced reached the V_{oc} requirements by a large margin, but had a surprisingly poor I_{sc}. At the same time we found a radio from Sangean that could operate at relatively low voltages (0.7–1.2 V) from a single rechargeable battery. The radio, however, required 9–9.8 mA at full power. We decided to connect the polymer solar cell modules to the battery through a 1N4148 diode that has a large voltage drop, but a very low reverse current. This was an important sacrifice to make as the battery would otherwise discharge through the solar cell in the absence of light as the typical resistance through the solar cell modules was in the 3–20 kΩ range (see Fig. 15). We distributed 205 FM radios at the festival powered by the best fraction of the devices prepared, and chose to bring many other electronic gadgets for the "Solar Hats" that could be powered entirely by the solar cell modules, that typically delivered around 1 mA and 2.2 V for the duration of the
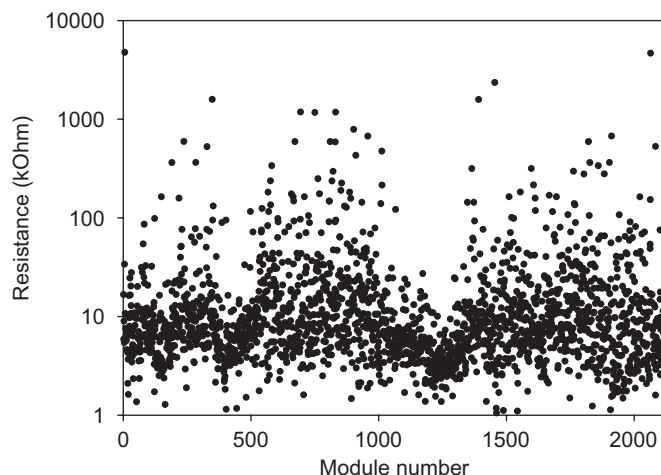

Fig. 15. The module resistance measured at zero bias for all the modules during production. A large range of values were observed with typical resistance in the rage 3–20 kΩ.

Fig. 16. The "Solar Hat" comprising hat, polymer solar cell, FM radio, ear plugs and neck strap (top left). Two large parasols were prepared for the festival each comprising 8 segments of 30–32 cells connected in parallel. The eight individual segments on the parasol could be connected in series or parallel (top right and middle). People innovating using the solar cells and a Sun-powered sewing machine.

festival. We had a workshop where visitors could assemble their own application from a limited choice of electronic gadgets. The most successful gadgets were the pocket calculator and the digital clocks. Fig. 16 shows some photographs from the festival under the collected theme "Rock the Climate", where aside from polymer solar cells, it was possible to run a sewing machine from silicon based solar cells. In the end the most successful part of this exercise was that visitors at the festival could bring their own ideas to life as exemplified by sewing a small bag with a polymer solar cells and a pocket calculator. There were many other good examples.

3.11. Future directions

An understanding of the interplay between production method and performance should be addressed through systematic studies of the printing techniques available and their combined use in preparing polymer solar cells. The aim should be towards vacuum free processing from solution using only roll-to-roll methods. A second direction is research into low-cost polymer materials that perform as well or nearly as well as the state of the art. A third direction is to devise complete processes to polymer solar cell

modules and their optimization with respect to the cost of the final product, which should be analyzed and scrutinized.

4. Conclusions

This report highlights the long stretch of technical research that need to be covered before the promises of polymer solar cells can be realized. A simple laboratory result based on a spin-coated solar cell does not in itself represent a promising technology. To be convincing, important issues such as stability, production methods and cost must be solved efficiently. It is obvious that the future work should focus on unifying stability, efficiency and process, and especially with respect to the latter it should be emphasized that a combination of R2R compatible printing techniques is probably the way towards the optimum polymer solar cells. We have shown that it is possible to transfer a laboratory result to industry, and have scaled it to full production scale and large area. The number of compromises that necessarily had to be made to meet the demanding objectives was so extensive that the success of the "Solar Hat" project should be rated as a failure, in the sense that the polymer solar cells could not fully power the lead application which was an FM radio. The project has, however, been successful in all other aspects where we demonstrated up-scaling of a laboratory result and transfer to actual industry conditions employing different film-forming techniques, etc. We have shown that it was possible to operate in a contaminated environment, but that it was necessary to carefully analyze the contaminants and thus avoid them by simple means. We used TOF-SIMS for this purpose and found that especially the ITO detaches in flakes from the surface and this leads to short circuits unless it is removed. Our results also confirm a good shelf life of the final product and an operational stability that met the requirement for a duration in excess of 1 week (or the length of the Roskilde Festival). Our industrial process allowed for a detailed analysis of the cost, and it is clear that the polymer solar cell technology must be processed fully by R2R processes employing the minimum of manual handling to become competitive in terms of process cost. In terms of materials cost there is a requirement for lower cost materials and a replacement of ITO in the transparent conductor.

Acknowledgements

Appendix A. Supplementary materials

Supplementary data associated with this article can be found in the online version at doi:10.1016/j.solmat.2008.12.001.

References

[1] C.J. Brabec, N.S. Sariciftci, J.C. Hummelen, Plastic solar cells, Adv. Funct. Mater. 11 (2001) 15–26.

[2] H. Spanggaard, F.C. Krebs, A brief history of the development of organic and polymeric photovoltaics, Sol. Energy Mater. Sol. Cells 83 (2004) 125–146.

[3] K.M. Coakley, M.D. McGehee, Conjugated polymer photovoltaic cells, Chem. Mater. 16 (2004) 4533–4542.

[4] H. Hoppe, N.S. Sariciftci, Organic solar cells: an overview, J. Mater. Res. 19 (2004) 1924–1945.

[5] C. Winder, N.S. Sariciftci, Low band gap polymers for photon harvesting in bulk heterojunctions solar cells, J. Mater. Chem. 14 (2004) 1077–1086.

[6] E. Bundgaard, F.C. Krebs, Low band gap polymers for organic photovoltaics, Sol. Energy Mater. Sol. Cells 91 (2007) 954–985.

[7] S. Günes, H. Neugebauer, N.S. Sariciftci, Conjugated polymer-based organic solar cells, Chem. Rev. 107 (2007) 1324–1338.

[8] M. Jørgensen, K. Norrman, F.C. Krebs, Stability/degradation of polymer solar cells, Sol. Energy Mater. Sol. Cells 92 (2008) 686–714.

[9] G. Li, V. Shrotriya, J. Huang, Y. Yao, T. Moriarty, K. Emery, Y. Yang, High-efficiency solution processable polymer photovoltaic cells by self-organization of polymer blends, Nat. Mater. 4 (2005) 864–868.

[10] W. Ma, C. Yang, X. Gong, K. Lee, A.J. Heeger, Thermally stable, efficient polymer solar cells with nanoscale control of the interpenetrating network morphology, Adv. Funct. Mater. 15 (2005) 1617–1622.

[11] J.Y. Kim, K. Lee, N.E. Coates, D. Moses, T.-Q. Nguyen, M. Dante, A.J. Heeger, Efficient tandem polymer solar cells fabricated by all-solution processing, Science 317 (2007) 222–225.

[12] F.C. Krebs, J. Alstrup, H. Spanggaard, K. Larsen, E. Kold, Production of large-area polymer solar cells by industrial silk screen printing, lifetime considerations and lamination with polyethyleneterephthalate, Sol. Energy Mater. Sol. Cells 83 (2004) 293–300.

[13] F.C. Krebs, H. Spanggaard, T. Kjær, M. Biancardo, J. Alstrup, Large area plastic solar cell modules, Mater. Sci. En. B 138 (2007) 106–111.

[14] C. Lungenschmied, G. Dennler, H. Neugebauer, N.S. Sariciftci, M. Glatthaar, T. Meyer, A. Meyer, Flexible, long-lived, large-area, organic solar cells, Sol. Energy Mater. Sol. Cells 91 (2007) 379–384.

[15] F.C. Krebs, H. Spanggaard, Significant improvement of polymer solar cell stability, Chem. Mater. 17 (2005) 5235–5237.

[16] F.C. Krebs, K. Norrman, Analysis of the failure mechanism for a stable organic photovoltaic during 10 000 h of testing, Prog. Photovoltaics Res. Appl. 15 (2007) 697–712.

[17] X. Yang, J. Loos, S.C. Veenstra, W.J.H. Verhees, M.M. Wienk, J.M. Kroon, M.A.J. Michels, R.A.J. Janssen, Nanoscale morphology of high-performance polymer solar cells, Nano Lett. 5 (2005) 579–583.

[18] E.A. Katz, S. Gevorgyan, M.S. Orynbayev, F.C. Krebs, Out-door testing and long-term stability of plastic solar cells, Eur. Phys. J. Appl. Phys. 36 (2006) 307–311.

[19] J.A. Hauch, P. Schilinsky, S.A. Choulis, R. Childers, M. Biele, C.J. Brabec, Flexible organic P3HT:PCBM bulk-heterojunction modules with more than 1 year outdoor lifetime, Sol. Energy Mater. Sol. Cells 92 (2008) 727–731.

[20] F.C. Krebs, Air stable polymer photovoltaics based on a process free from vacuum steps and fullerenes, Sol. Energy Mater. Sol. Cells 92 (2008) 715–726.

[21] F.C. Krebs, Y. Thomann, R. Thomann, J.W. Andreasen, A simple nanostructured polymer/ZnO hybrid solar cell—preparation and operation in air, Nanotechnology 19 (2008) 424013.

[22] M. Bjerring, J.S. Nielsen, A. Siu, N.C. Nielsen, An explanation for the high stability of polycarboxythiophenes in photovoltaic devices—a solid-state NMR dipolar recoupling study, Sol. Energy Mater. 92 (2008) 772–784.

[23] J.S. Liu, E.N. Kadnikova, Y.X. Liu, M.D. McGehee, J.M.J. Fréchet, Polythiophene containing thermally removable solubilizing groups enhances the interface and the performance of polymer–titania hybrid solar cells, J. Am. Chem. Soc. 126 (2004) 9486–9487.

[24] F.C. Krebs, R.B. Nyberg, M. Jørgensen, Influence of residual catalyst on the properties of conjugated polyphenylenevinylene materials: palladium nanoparticles and poor electrical performance, Chem. Mater. 16 (2004) 1313–1318.

[25] K.T. Nielsen, K. Bechgaard, F.C. Krebs, Removal of palladium nanoparticles from polymer materials, Macromolecules 38 (2005) 658–659.

[26] K.T. Nielsen, K. Bechgaard, F.C. Krebs, Effective removal and quantitative analysis of Pd, Cu, Ni, and Pt catalysts from small-molecule products, Synthesis (2006) 1639–1644.

[27] K.T. Nielsen, P. Harris, K. Bechgaard, F.C. Krebs, Structural study of four complexes of the $M-N_2S_2$ type derived from diethylphenylazothioformamide and the metals palladium, platinum, copper and nickel, Acta. Crystallgr. B 63 (2007) 151–156.

[28] F.C. Krebs, M. Jørgensen, Decomposable vehicles in printing or coating compositions, (filing date 13.04.2007), WO2007118850 A1.

[29] M. Jørgensen, O. Hagemann, J. Alstrup, F.C. Krebs, Thermo-cleavable solvents for printing of conjugated polymers: application in polymer solar cells, Sol. Energy Mater. Sol. Cells 93 (2009) 413–421.

[30] H. Womelsdorf, W. Hoheisel, G. Passing, Nanopartikuläres, redispergierbares fällungsoxid, German Patent (filing date 23.02.1999), DE 19907704 A1.

[31] H. Womelsdorf, W. Hoheisel, G. Passing, Process for producing nanoparticulate, redispersible zinc oxide gels, European Patent (filing date 11.02.2000) EP 1157064 B1.

[32] H. Womelsdorf, W. Hoheisel, G. Passing, Nanoparticulate, redispersible zinc oxide gels, United States Patent (patent date 23.03.2004) US 6,710,091 B1.

[33] W.J.E. Beek, M.M. Wienk, M. Kemerink, X. Yang, R.A.J. Janssen, Hybrid zinc oxide conjugated polymer bulk heterojunctions solar cells, J. Phys. Chem. B 109 (2005) 9505–9516.

[34] S.A. Gevorgyan, M. Jørgensen, F.C. Krebs, A setup for studying stability and degradation of polymer solar cells, Sol. Energy Mater. Sol. Cells, 92 (2008) 736–745.

[35] S.E. Shaheen, R. Radspinner, N. Peyghambarian, G.E. Jabbour, Fabrication of bulk heterojunction plastic solar cells by screen printing, Appl. Phys. Lett. 79 (2001) 2996–2998.

[36] T. Aernouts, P. Vanlaeke, J. Poortmans, P. Heremans, Polymer solar cells: screen printing as a novel deposition technique, Proc. SPIE 5464 (2004) 252.

[37] J.C. Vickerman, D. Briggs, TOF-SIMS Surface Analysis by Mass Spectrometry, IM Publications and Surface Spectra Limited, West Sussex, 2001.

[38] B. von Roedern, H.S. Ullal, The role of polycrystalline thin-film PV technologies in competitive PV module markets, in: 33rd IEEE Photovoltaic Specialists Conference, 2008, NREL/CP-520-42494, pp. 1–4.

[39] M. Glatthaar, M. Riede, N. Keegan, K. Sylvester-Hvid, B. Zimmermann, M. Niggemann, A. Hinsch, A. Gombert, Efficiency limiting factors of organic bulk heterojunction solar cells identified by electrical impedance spectroscopy, Sol. Energy Mater. Sol. Cells 91 (2007) 390–393.

[40] A.S. da Silva Sobrinho, M. Latrèche, G. Czeremuszkin, J.E. Klemberg-Sapieha, M.R. Wertheimer, Transparent barrier coatings on polyethylene terephthalate by single and dual-frequency plasma-enhanced chemical vapour deposition, J. Vac. Sci. Technol. A 16 (1998) 3190–3198.

[41] M. Andersen, J.E. Carlé, N. Cruys-Bagger, M.R. Lilliedal, M.A. Hammond, B. Winther-Jensen, F.C. Krebs, Transparent anodes for polymer photovoltaics: oxygen permeability of PEDOT, Sol. Energy Mater. Sol. Cells 91 (2007) 539–543.

[42] T. Aernouts, P. Vanlaeke, W. Geens, J. Poortmans, P. Heremans, S. Borghs, R. Mertens, R. Andriessen, L. Leenders, Printable anodes for flexible organic solar cell modules, Thin Solid Films 451–452 (2004) 22–25.

[43] M. Strange, D. Plackett, M. Kaasgaard, F.C. Krebs, Biodegradable polymer solar cells, Sol. Energy Mater. Sol. Cells 92 (2008) 805–813.

[44] K.-Y. Lee, S.T. Connor, Y. Cui, P. Peumans, Solution-processed metal nanowire mesh transparent electrodes, Nano Lett. 8 (2008) 689–692.

[45] ⟨http://www.roskilde-festival.dk/2008/frontpage⟩.

[46] M. Niggemann, B. Zimmermann, J. Haschke, M. Glatthaar, A. Gombert, Organic solar cell modules for specific applications—from energy autonomous systems to large area photovoltaics, Thin Solid Films 516 (2008) 7181–7187.

[47] F.C. Krebs (Ed.), Polymer Photovoltaics: A Practical Approach, SPIE Press, Bellingham, 2008, pp. 71–72.

[48] A.R. Murphy, J. Liu, C. Luscombe, D. Kavulak, J.M.J. Fréchet, R.J. Kline, M.D. McGehee, Synthesis, characterization, and field-effect transistor performance of carboxylate-functionalized polythiophenes with increased air stability, Chem. Mater. 17 (2005) 4892–4899.

[49] F. Verbakel, S.C.J. Meskers, R.A.J. Janssen, Electronic memory effects in diodes from a zinc oxide nanoparticle-polystyrene hybrid material, Appl. Phys. Lett. 89 (2006) 102103.